EFFECTS OF TITANIUM OXIDE (TiO$_2$) ON THE PHYSICAL, MECHANICAL AND MICROSTRUCTURE PROPERTIES OF ALUMINA

WAI JIE SHENG

A project report submitted in partial fulfilment of the requirements for the award of Bachelor of Engineering (Hons.) Mechanical Engineering

Faculty of Engineering and Science

Universiti Tunku Abdul Rahman

May 2011

DECLARATION

I hereby declare that this project report is based on my original work except for citations and quotations which have been duly acknowledged. I also declare that it has not been previously and concurrently submitted for any other degree or award at UTAR or other institutions.

Signature : _____

Name   : Wai Jie Sheng_____

ID No.   : 07UEB07778_____

Date   : _____

APPROVAL FOR SUBMISSION

I certify that this project report entitled **"EFFECTS OF TITANIUM OXIDE, TiO$_2$ ON THE PHYSICAL, MECHANICAL AND MICROSTRUCTURE PROPERTIES OF ALUMINA"** was prepared by **WAI JIE SHENG** has met the required standard for submission in partial fulfilment of the requirements for the award of Bachelor of Engineering (Hons.) Mechanical Engineering at Universiti Tunku Abdul Rahman.

Approved by,

Signature : _____

Supervisor : Mr. Ting Chen Hunt

Date   : _____

The copyright of this report belongs to the author under the terms of the copyright Act 1987 as qualified by Intellectual Property Policy of University Tunku Abdul Rahman. Due acknowledgement shall always be made of the use of any material contained in, or derived from, this report.

ACKNOWLEDGEMENTS

I would like to thank everyone who had contributed to the successful completion of this project. Particularly, I would like to express my gratitude to my research supervisor, Mr. Ting Chen Hunt for his invaluable advice, guidance and his enormous patience throughout the development of the research. Under his supervision, the final year project can be proceeded in accordance to the planned schedule. Besides, I am thankful to UTAR and all the laboratory assistants for providing various intruments and equipments for final year project students for testing purpose.

Furthermore, the assistance of Ms. Zoey Kang, who had spent her valuable time in performing the X-ray diffraction (XRD) and grain size inspection of the tested samples through Scanning Electron Microscope (SEM), is much appreciated. Besides, I am grateful to other members of similar final year project title, who are Cheng Chuen Rong, Choo Wei Seng, Lim Wee Keat, Tan Ye Lock and Yong Chan Han for their knowledge sharing, tolerance and coorperation given from the beginning until the completion of of the project.

EFFECTS OF TITANIUM OXIDE, TiO$_2$ ON THE PHYSICAL, MECHANICAL AND MICROSTRUCTURE PROPERTIES OF ALUMINA

ABSTRACT

The influence of Titanium Oxide (TiO$_2$) on the densification and grain growth of alumina ceramics, Al$_2$O$_3$ at a low sintering temperature was investigated. In this study, samples was prepared by a series of processes such as uniaxial pressing, cold isostatic pressing (CIP) and pressureless sintered in air at temperature ranging from 1250°C to 1450°C. The sintered bodies were examined with different testings to determine the bulk density, hardness, Young's modulus, grain size as well as the presence of its secondary phase. The study revealed that the maximum value of 3.822 g/cm^3 can be attained by sample doped with 0.5 wt.% TiO$_2$ at 1450°C as the bulk density increases with increasing sintering temperature. Both Young's modulus and hardness were found to be increased with the addition of 0.5 wt.% TiO$_2$. It was also observed that the 0.5 wt.% TiO$_2$ is optimal in exhibiting the highest Young's Modulus of 267.74 GPa and maximum Vickers hardness of 7.6 GPa at 1450°C if compared to that of the undoped alumina which obtained 20.61 GPa and 1.79 GPa, respectively under the same temperature. At 3.0wt.% of TiO$_2$ addition and at 1450°C of sintering temperature, the formation of secondary phase of Al$_2$TiO$_5$, which has a low elastic moduli as compared to alumina, reduces the hardness of the sintered bodies to 5.34 GPa. The grain growth is shown to be promoted simultaneously after TiO$_2$ addition up to 1.5 wt.% of concentration. The largest average grain size, 1.03 μm, and the largest grain recorded, 2.48 μm, were found to be occurred at 1.5 wt.% TiO$_2$ when sintered at 1450°C. The appearance of intragranular pores was found in sample with higher addition levels of dopants such as 5.0 wt.% TiO$_2$ at 1450°C whereas the intergranular pores, at the same temperature, were reduced significantly as noticed in 0.5 wt.%, 1.5 wt.% and 3.0 wt.% TiO$_2$ doped alumina, thus leads to a relatively uniform grain size distribution.

TABLE OF CONTENTS

CHAPTER

LIST OF TABLES

LIST OF FIGURES

LIST OF SYMBOLS / ABBREVIATIONS

ρ	Bulk density of the sample
W_a	Weight of the sample in air
W_w	Weight of the sample in water and
ρ_w	Density of the distilled water which vary with temperature
E	Young's Modulus (Pa)
m	Mass of the rectangular bar (g)
b	Width of the bar (mm)
L	Length of the bar (mm)
t	Thickness of the bar (mm)
F_f	Fundamental resonant frequency of bar in flexure, (Hz)
T_1	Correction factor for fundamental flexural mode to account for finite thickness of bar, Poisson's ratio etc.
P	Applied load
D	Average diagonals
μ	Poisson's ratio

LIST OF APPENDICES

CHAPTER 1

INTRODUCTION

1.1　Background

In recent years, many researches have been carried out to refine the physical, mechanical and microstructural properties of alumina that is known for its porosity. Actually, porosity can be effectively reduced by attaining high densities and maintaining fine grains of alumina throughout the sintering process. However, the desired result was seldom achieved due to the inherent phenomenon of grain coarsening when alumina ceramics are sintered at elevated temperature. On the other hand, a high sintering temperature is necessary to achieve high densification of alumina which is comparable to its theoretical density. Therefore, this has led to the dilemma in which either one of the desired properties have to be compromised in order to obtain the optimal result of another.

The topic on alumina ceramics is of scholars' interests due to its availability, low cost and desired properties such as high melting temperature, high hardness, wear resistance, chemical stability and other characteristics which are advantageous for structural applications. Hence, the improvement of alumina properties is crucial because it is directly associated with the reliability of the potential applications. Also, it is rational to conduct such research for academic purpose so that more students can keep attentive to the latest development of alumina ceramics. However, several limitations of the research have emerged as a result of resources and facilities deficiency. For instance, microwave sintering, which produces homogeneous microstructure at a lower sintering temperature via uniform heat dissipation, could

not be performed due to the lack of devices and equipments. Likewise, cold isostatic pressing, which yields a higher green density of the powder compact, is required to be carried out by using the facilities in other universities.

1.2   Aims and Objectives

This final year project is aimed to identify the effects of Titanium Oxide, TiO_2 addition on alumina ceramics in the aspects of physical, mechanical, microstructural properties throughout the hands on practices. In the interim, the objectives will be focused on lowering the sintering temperature while achieving relatively high densification of alumina, Al_2O_3 at the same time. Besides, the improvement of densification should be attained without compromising of the grain growth in an attempt to preserve a uniform distribution of fine grains of Al_2O_3.

1.3   Thesis Structure

This final year project encompasses introduction, literature review, results, discussion, conclusion and recommendations.

CHAPTER 2

CERAMICS

2.1 Definition

In fact, the word "Ceramic" is originated from the term "*Keramikos*", which signifies burnt material in Greek expression. In other words, it describes the articles made by using muds and water with subsequent sun drying and furnace blazing during the ancient times. According to the late Father of Modern Ceramic Engineering, Dr. W. David Kingery, ceramic is any substance that is inorganic and non metallic in nature. By definition, ceramic materials are regarded as neither metallic nor non metallic elements but an intermediate compounds between the two constituents. This is because ceramic is formed by the combination of both metallic and non metallic solid elements under the application of heat treatment, which is known as firing or sintering. Most of the ceramic materials are existing in the form of oxides, carbides, and nitrides (Carter and Norton, 2007).

Figure 2.1: Porcelain pottery, Clay bricks and Ceramic Tiles

2.2   History and Evolution of Ceramics

The chronology of ceramic can be traced back to 24,000 BC when the first sacred statue was discovered. Due to the emergence of civilization in 10,000 years later, many clay related products such as bricks, tiles and pottery containers were uncovered. When it came to 8,000 BC, pottery with coloured glaze were produced by the Egyptians through the overheating process in the kiln that was partially grounded. During the advent of industrial revolution in 16th century, refractory materials that possess a better resistant to high temperature were developed to serve as lining materials of furnace, which replaced the conventional grounded kilns to melt the metals and glasses in industrial scale (American Ceramic Society [ACS], 2010).

In modern ages, a variety of advanced ceramic materials, such as magnetic ceramics and optical ceramics, were created via various refinement approaches to overcome the limitations of traditional ceramics for which the primary raw material is clay. These advanced ceramics may consist of oxides, carbides or materials which do not constitute any natural counterparts. The improvement of advanced ceramics in the aspects of mechanical, electrical and physical properties had benefited a wide range of industries such as aeronautics, medical, automobile and semiconductor manufacturing (ACS, 2010).

2.3   Types of Ceramics

Ceramic materials can be categorized into two different types, which are crystalline and non crystalline ceramics. Most of the ceramic materials exist in crystalline form where all atoms are located within well defined locations to establish an atomic arrangement that repeats uniformly over the structure. Typical examples of crystalline ceramics are aluminium oxide, sodium chloride and magnesium oxide. In the interim, non crystalline ceramics or amorphous ceramics, are composed of a short range order of atoms in the crystal structure in which the positions of atoms are scattered instead of regular arrays. For instance, some of the representatives of non crystalline ceramics are glass and glass-ceramics (Roush et al., 2000).

2.4   Crystal Structures of Ceramics

In general, ceramics exhibit a wider variety of crystal structure which is more sophisticated if compared to those of the metals that are mainly comprised of face-center cubic (FCC), body-centered cubic (BCC) or hexagonal closed-packed (HCP). By definition, ionic bonding is the transfer of both oppositely charged ions from one atom to another by the means of electrostatic forces to attain octet condition. Meanwhile, covalent bonding involves the sharing of electrons between two elements to achieve stable configuration (Callister, 2007).

Primarily, the atomic bonding of most ceramics consists of the combination of both ionic and covalent types in which the extent of ionic character is mainly influenced by the eletronegativities of the atoms. For instance, table 2.1 summarizes the degree of ionic character to show the dominance of bonding for each type of ceramic materials. From the table, it can be shown that the chemical bonding of calcium fluoride and magnesium oxide are predominantly ionic whereas silicon carbide and zinc sulfide are primarily covalent bonded (Callister, 2007).

Table 2.1: Degree of Ionic Character of Different Ceramic Materials (Callister, 2007).

Materials	Chemical formula	Ionic character (%)
Calcium Fluoride	CaF_2	89
Magnesium Oxide	MgO	73
Sodium Cloride	$NaCl$	67
Aluminium Oxide	Al_2O_3	63
Silicon Oxide	SiO_2	51
Silicon Nitride	Si_3N_4	30
Zinc Sulfide	ZnS	18
Silicon Carbide	SiC	12

Actually, the main criterion of a crystal structure is to ensure the neutrality of the charges. In other words, the amount of all the positive cation must be equivalent to that of the negative anion so that balance of the charges can be in equilibrium .Theoretically, the ionic radii of the positive cations will be smaller than the negative cations due to the electron which is donated by the metallic elements to the non-metallic elements during the ionization. In fact, the crystal structure of ceramics is considered stable when the cation remains intact with all the surrounded anions as shown in Figure 2.2 (Callister, 2007).
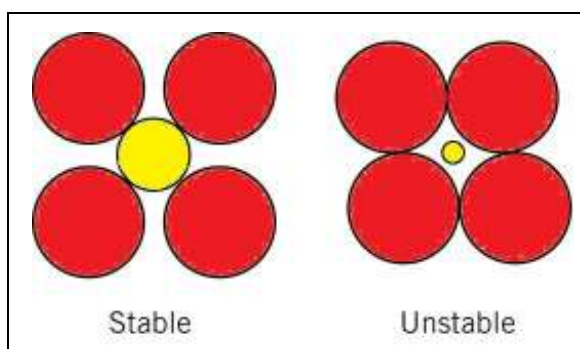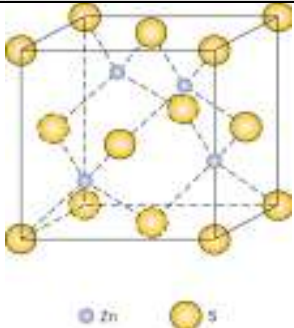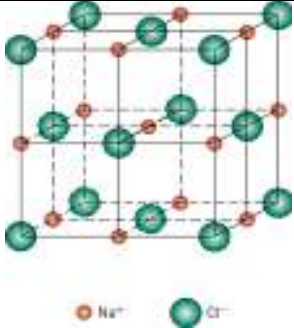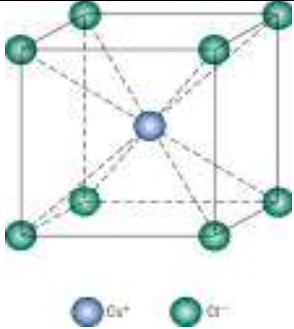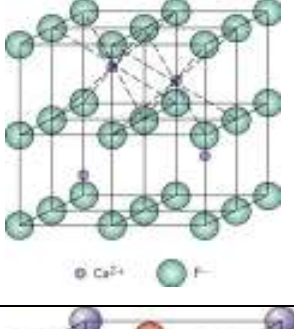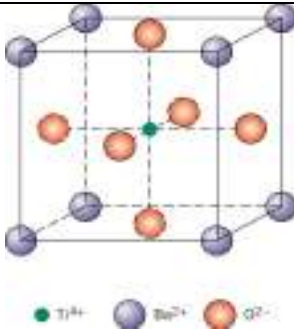
Figure 2.2: Stable and Unstable Anion-Cation Coordination Configuration
Red circles denotes anions ; Yellow circles indicates cations.

Crystal structure of ceramics can be generally classified into three categories, which are AX-type, A_mX_p-type and $A_mB_nX_p$-type where A indicates the cations and X represents the anions. With regard to the AX compounds, the number of cations and anions are equal within the crystal structure. In contrast, the charges on the cations and anions are unequal in the case of A_mX_p compounds, which implies that the amount of cations and anions will be different in the structure. Meanwhile, there can be more than a single cation exists within a crystal structure, which yields the chemical formula of $A_mB_nX_p$. Table 2.2 summarizes different crystal structure for some of the common ceramic materials (Callister, 2007).

Table 2.2: Summary of Some Common Ceramic Crystal Structures (Shackelford, 2009).

Structural Type	Structural Name	Unit Cell	Examples
AX	Zinc Blende (Sphalerite)		ZnS, SiC
	Sodium Chloride (Rock Salt)		NaCl, MgO, FeO
	Cesium Chloride		CsCl
AX_2	Flourite		CaF_2, UO_2, ThO_2
ABX_3	Perovskite		$BaTiO_3$, $SrZrO_3$, $SrSnO_3$

2.5 Microstructure of ceramics

Indeed, microstructure plays an essential role in determining the final properties of the ceramic materials. In the case of crystalline ceramics, the microstructure is formed by polycrystalline solids that comprised of a collection of many single crystals, which are called as grains. These grains are separated by the grain boundaries, which alter the crystal lattice orientation from one grain to another as shown in Figure 2.3 (Barsoum, 2003).
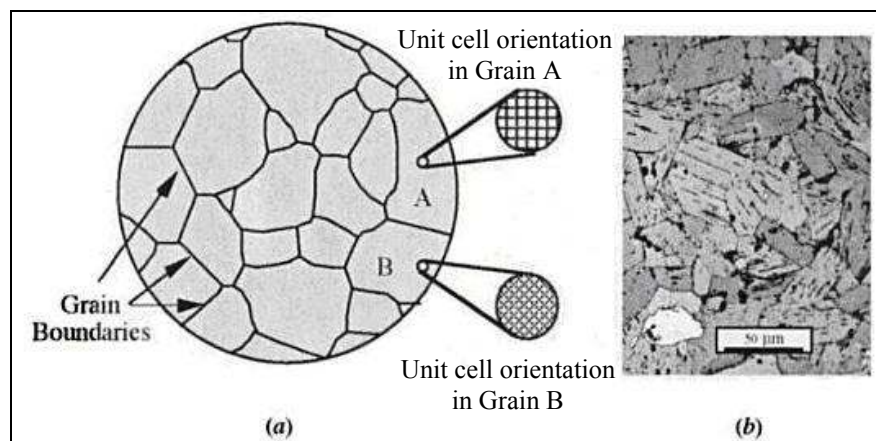
Figure 2.3: (a) Schematic of Polycrystalline Sample (b) Microstructure Observed Under The Microscope (Barsoum, 2003).

In actual fact, physical, mechanical, and functional properties of the ceramics are greatly influenced by the size, shapes and orientation of the grain as well as porosity within microstructure. For instance, smaller grain size may yield a stronger and denser microstructure, which will further lead to a greater size of grain boundary that is capable of impeding the dislocation motion throughout the entire structure. Typically, the use of microscope is necessary to observe the grain size of ceramics which are ranged from 1 to 50 μm (Rice et al., 2000).

However, a well dispersed of grain size distribution is hardly to be seen in the microstructure of the ceramic materials. This is owing to the inherent presence of imperfections such as pores, micro cracks, notches which will deteriorate the final properties of the ceramic materials. Unlike the metals, ceramics would have

approximately 20% of porosity within its microstructure which should be treated by various processing methods such as sintering. Apart from that, it is apparent to have more than a single phase to present in the microstructure of ceramics due to the reason that ceramics are formed by at least two elements. For that, each phase would have their distinctive structure, composition and properties which are varied from one to another (Brevier Technical Ceramics [BTC], 2004).
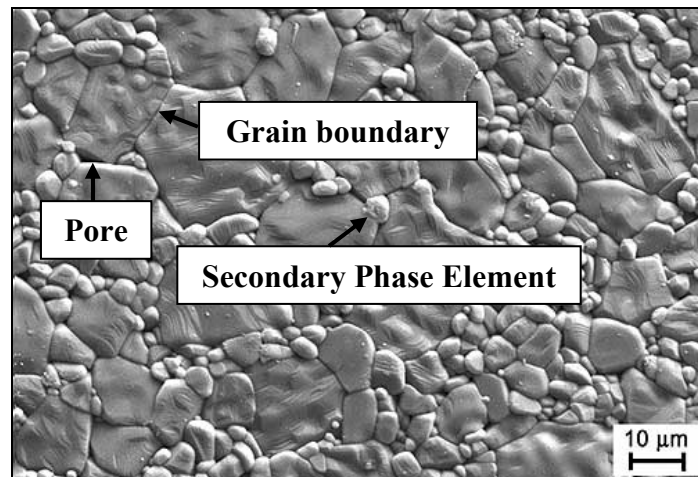
Figure 2.4: Microstructural Features of Alumina, Al$_2$O$_3$ (BTC, 2004).

2.6 Ceramics Properties

Normally, the public may have perception that ceramics are inferior materials due to its unfavourable mechanical properties such as brittleness, poor heat and electricity conductivities and non magnetism. Due to this preconceived notion, they prefer metals or other stronger materials which are more ductile, magnetic, thermally and electrically conductive in selecting the raw materials for various applications such as automobile manufacturing and military usages. In fact, certain traditional ceramics and the emergence of advanced ceramics have overthrown the universal understanding of ceramics since they possess a better combination of physical, mechanical and functional properties which are comparable to that of the metals (Richerson, 2006).

2.6.1   Mechanical properties

Typically, the applications of ceramics are constrained due to its inherent brittleness that is susceptible to fracture under the tensile stresses. This can be verified by both crystalline and non crystalline ceramics which tend to fail immediately upon the application of tensile load before experiencing any plastic deformation at the room temperature. In fact, ceramics comprise of ionic and covalent bonding which are rigid rather than metallic bonding that allows the occurrence of slip mechanism, which is essential in providing the tolerance for materials to deform plastically. Hence, the stiff bonding makes ceramics incapable to withstand any plastic deformation before brittle failure occurs (Richerson, 2006).

Ceramics are well known of their high hardness, excellent wear resistance and low fracture toughness. In other words, ceramics are much less susceptible to wear and erosion due to their good tribological properties, which provide a prolonged service life of an application. In the interim, ceramics have low fracture toughness which is analogous to that of the polymers. In fact, low fracture toughness is one of the characteristics that is associated with the brittle materials. Hence, internal cracks in ceramic materials will cause the occurrence of brittle fracture when they are subjected to any additional loading (Richerson, 2006).
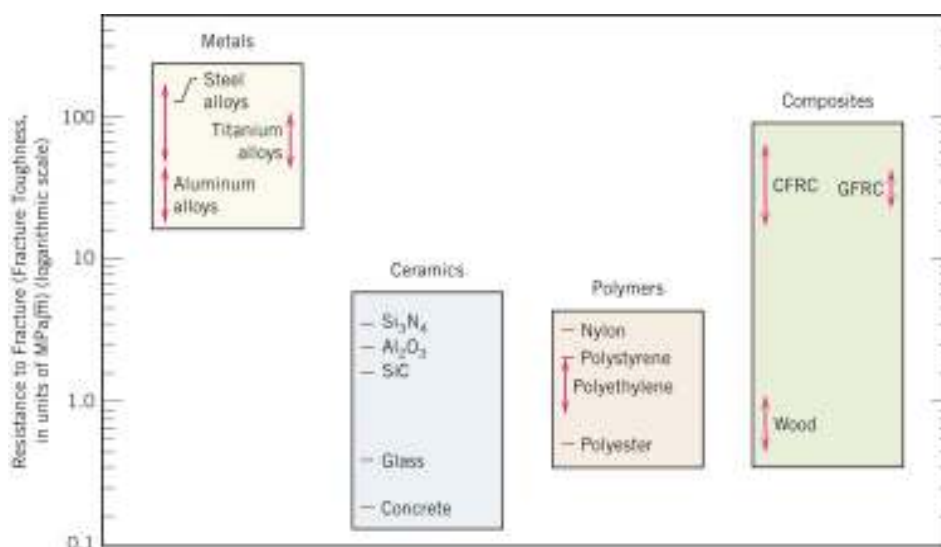
Figure 2.5: Comparison of Fracture Toughness Between Different Materials (Callister, 2007).

Besides, the presence of defects such as microvoids, cracks and internal flaws in ceramics readily serve as the stress concentration points that amplify the crack propagation and lead to the brittle fracture when they are subjected to impact loading. Furthermore, creep deformation of ceramic materials occurs under the exposure of both elevated temperature and static mechanical stresses. Unlike the brittle fracture, this deformation is time dependent because it is initiated by the strain which is accumulated from the long term exposure of stresses (Richerson, 2006).

Owing to the molecular structure, ceramic materials have comparatively low flexural strength as they tend to rupture under the exertion of bending and tensile forces. For instance, most of the ceramics fail after they were subjected to around 0.1 % of strain. On the other hand, the molecular structure of ceramics enables it to own a high degree of compressive strength although it is relatively fragile under tensile stresses. For example, porcelain will be a good representative of ceramics which can withstand a compressive load that is ten fold larger than its tensile strength. This advantage has extended the usage of ceramics to the fabrication of concrete composed of Portland cements, which is one of the branches of ceramics that contains high compressive strength (Callister, 2005).

2.6.2   Physical Properties

As shown in Figure 2.6, most of the ceramic materials are less dense than the metals but denser if compared to polymers and composites. This implies that ceramics are actually lighter than metal while heavier than polymers and composite. Therefore, ceramics are the popular materials to be used in the fabrication of automobile and aircraft engines which are emphasizing on the aspect of lightweight. As similar to polymers, electrical conductivities of most ceramics are relatively lower if compared to that of the metals. However, ceramics have a greater range of electrical conductivities values, which allows ceramics to be used as insulator as well as electrical conductors due to their inherent insulative and conductive effects (Groover, 2010).
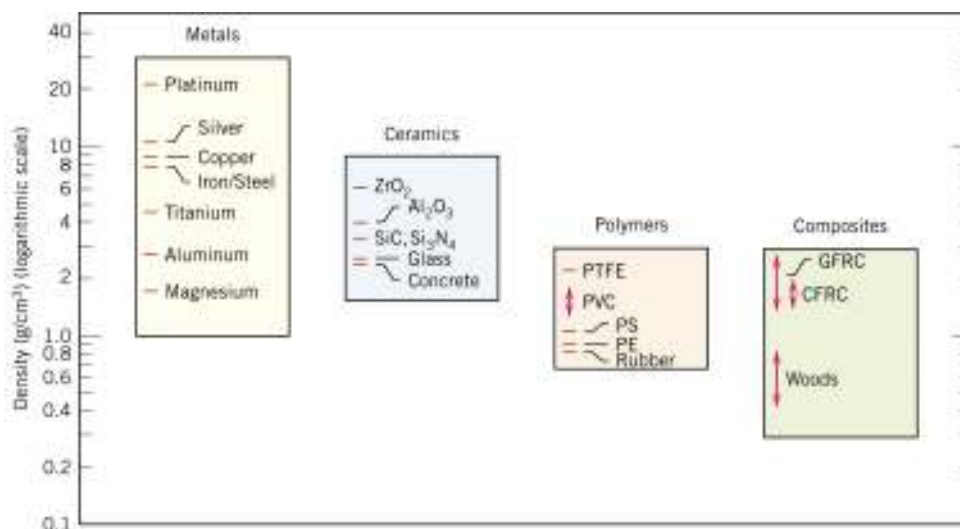
Figure 2.6: Comparison of Density Between Different Materials (Callister, 2007).

In fact, ceramic materials are resistant to high temperature due to their high melting point which are much higher than that of most metals. Therefore, they have been widely used in various high temperature applications. Nevertheless, some ceramics tend to decompose instead of melting under the exposure of high temperature. For instance, Silicon Nitride (Si_3N_4) tends to decay under high temperature due to its amorphous nature. As a result, sintering of Si_3N_4 under high pressure of nitrogen is required to inhibit the decomposition from happening (Callister, 2007).

Similarly, thermal expansion coefficients of ceramics is smaller than the metals' but minute effect of expansion may be detrimental to ceramic materials due to their intrinsically brittleness. For instance, thermal shock, or simply thermal cracking is a typical phenomenon that particularly occurs in ceramic materials with high thermal expansions and low thermal conductivities. Under high temperature, these properties will result in significant temperature gradients that bring different regions of the ceramic materials to expand unevenly. With that, borosilicate glass ceramics, Pyrex with reduced coefficient of thermal expansion and greater strength was developed to overcome the effect of thermal cracking (Groover, 2010).

2.6.3   Functional Properties

Generally, functional properties of ceramics can be classified into optical, magnetic and chemical aspects. From optical perspective, ceramic materials exhibit their light transmittance features such as opaque, translucency and transparency through the removal of residual pores and microstructure homogeneity. Meanwhile, some of the oxide ceramics such as Ferum oxide, Fe_3O_4, can behave magnetically, thus leads to a increased usages in applications which are mainly predominated by the metals. Most of the ceramics are inert to chemical reactions in which they resist oxidation and corrosion. As a result, ceramic materials would possess a longer lifetime than metals and polymers due to its chemical resistance in hostile environment that contains moisture and other reactive chemical substances (Pfeifer, 2009).

2.7   Classification of Ceramics Based On Applications

Ceramics materials can be grouped into six major families, which are glasses, clay products, refractories, abrasives, cements and advanced materials. Each of them possess unique properties that are suitable for certain applications. Besides, most of the ceramic materials are further processed with specific composition and different sintering approches to enhance their usability. For instance, fireclay, silica, basic and special refractories are formed from the base refractory ceramics to serve for different functions in the furnace construction (Callister, 2007).
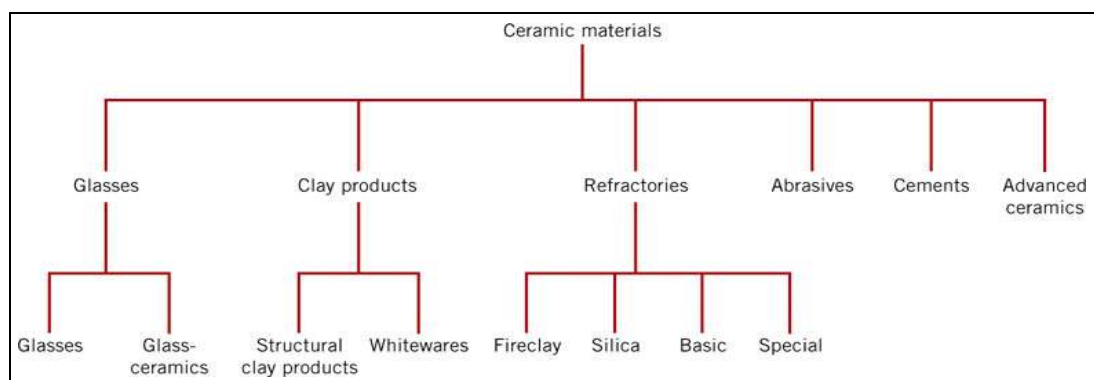
Figure 2.7: Comparison of Density Between Different Materials (Reh, 2007).

Table 2.3: Types of Ceramic Materials And Their Applications (Carter and Norton, 2007).

Ceramics Materials	Characteristics	Applications
Glasses ▪ Glasses ▪ Glass-ceramics	▪ Optical transparency ▪ High mechanical strength ▪ Low thermal expansion coefficients ▪ Resistant to high temperature ▪ Excellent dielectric properties	o Container, lenses and fiberglass
Clay products ▪ Structural Clay Products ▪ Whiteware	• High structural integrity • Non plastic • Colour turns white after high temperature firing.	o Building bricks, tiles, sewer pipes, porcelain, pottery, tableware, china plumbing fittings.
Refractories ▪ Fireclay ▪ Silica ▪ Basic ▪ Special	• Thermally insulative • High temperature load-bearing capacity • Resistant to slags • Susceptible to oxidation at high temperature • Electrical resistance	o Steel arched roof, steel making open hearth furnaces and furnace components
Abrasives	• High hardness • Wear resistance • High toughness	o Sand paper, cutter and grinder
Cements	• Binds composite materials into a coesive mass or aggregates of inert particles.	o Mortar, concrete, plaster of Paris
Advanced Ceramics	• Highly refined ceramics with enhanced physical, functional and mechanical attributes.	o Optical fibers and ceramic ball bearings

CHAPTER 3

ALUMINA

3.1   Introduction

Alumina, also known as Aluminium Oxide (Al_2O_3), is a ceramic compound which appears in white or nearly transparent colour in nature. The colourless appearance of alumina is attributed to the absence of metal impurities in its composition. Alumina exists inherently as corundum or in gemstone form such as ruby and sapphire, which having metal consituents that offer dyeing to their appearance (Heimke, 1990).

Meanwhile, alumina can be formed from the bauxite ore, which is a hydrous aluminium oxide that consists of gibbsite, $Al(OH)_3$, boehmite, γ-AlO(OH) and diaspore, α-AlO(OH). From the bulk of bauxite, pure alumina can be extracted by the Bayer process, which is an approach to remove water from bauxite through a series of actions. In this process, bauxite is milled and digested with heated caustic liquor, sodium hydroxide, NaOH to form aluminium hydroxide, $Al(OH)_3$. Upon cooling, the mixture starts to crystallize and precipitate. Finally, pure alumina can be produced by performing calcination to $Al(OH)_3$ for water removal (Rice, 2003).

Figure 3.1: Alumina Powders

3.2 Microstructure of Alumina

3.2.1 Transition Phase of Alumina

Indeed, the formation of intermediate metastable alumina phases such as gamma (γ), theta (θ), epsilon (ε), chi (χ), eta (η), delta (δ), kappa (κ) and iota (ι) are necessary to shape the thermal end product, the stable phase of crystalline α-alumina upon the heating temperature of 1000°C. In this process, any transition phase will develop into another transition with different crystalline structure when the temperature is increased. Noticeably, the series of phase changes leading to the α-alumina is irreversible and each phase transformation acts sluggishly and occurs over a broad range of sintering temperature (Carniglia and Barna, 1992).
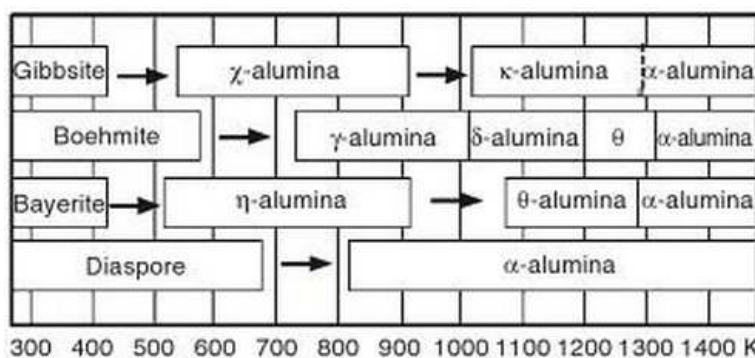
Figure 3.2: Transformation Sequence From Al(OH)₃ to Al₂O₃ (Heimann, 2010).

As shown in Figure 3.2, the sequential order in which transition alumina takes place relies on the starting materials such as boehmite, gibssite and diaspore. Under heating process, boehmite will be transformed into γ-phase at around 730°C, δ-phase at 1010°C, θ-phase at 1200°C and finally reaches α-phase at 1310°C. Conversely, the transition phase for gibbsite occurs with the succession from χ-phase, κ-phase to α-phase Al_2O_3 at 540°C, 1020°C and 1300°C, respectively. Unlike boehmite and gibbsite, diaspore transforms directly to α-Al_2O_3 at around 820°C. Along the phase development from hydrated compounds, transition aluminas are highly susceptible to porosity in its microstructure due to the partially disordered lattice arrangement (Lee and Rainforth, 1994).

3.2.2 Crystal Structure of Transition Aluminas

From crystallographic aspect, each transition phase of alumina has their distinctive crystal structure as shown in Table 3.1. However, α-alumina, or simply corundum in its natural form, is dissimilar to its transition phases as it requires the transformation of crystal structure from face centered cubic (FCC) to hexagonal close packing (HCP). In other words, the crystal structure of α-alumina involves the packing of oxygen ions in a close-packed hexagonal arrangement with aluminium ions in two-thirds of the octahedral sites (Carniglia and Barna, 1992).

Table 3.1: Various Transition Phases of Alumina and Their Crystal Structure (Heimann, 2010).

Transition Phase	Symbol	Crystal Structure
Gamma	γ	Cubic
Eta	η	Cubic
Chi	χ	Hexagonal
Delta	δ	Tetragonal
Theta	θ	Monoclinic
Kappa	κ	Orthorhombic
Epsilon	ε	Hexagonal

Besides, the partially disordered crystal structures of transition alumina are strongly dependent on the closed-packed oxygen sublattice with varying interstitial aluminium configurations. However, the crystal structures tend to approach the formation of hexagonal oxygen sublattice with elevated heating temperature up to the point where the formation of stable α-alumina is completed (Lee et al., 1994).
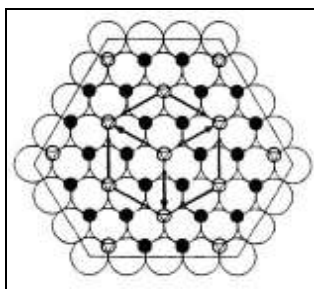
Figure 3.3: The Hexagonal Close Packed Crystal Structure of Alumina (Jacobs et al., 1998).

3.3   Properties of Alumina

3.3.1   Physical Properties

In fact, alumina is favourable for its low density, 3.98 g/cm^3, which makes alumina lighter in weight if compared to that of the metals. Likewise, the capability of alumina in withstanding the temperature variation is owing to its inherent specific heat capacity of 774.977 J/kg.K that allows the body to adapt with the temperature fluctuations at outer environment. Besides, the low thermal conductivities of alumina, which is ranging from 10 to 40 Wm/K, enables it to withstand extreme temperature and resistive to any heat transfer (Black and Hastings, 1998).

Moreover, alumina owns some excellent thermal properties at the room temperature. For instance, alumina has a high melting point of 2053 K; nevertheless, the melting temperature may be lowered considerably by the presence of impurities or other alloying elements in alumina that form the secondary phases (Black and Hastings, 1998). Other physical properties of single crystal α-alumina and their respective values are shown in the Table 3.2.

Table 3.2: Physical Properties of Single Crystal α-Alumina
(Riedel and Chen, 2000).

Physical Properties	Value	Unit
Density	3.98	g/cm^3
Specific Heat Capacity	774.977	J/kg.K
Thermal Conductivities	40 (25°C) 10 (1000°C)	Wm/K
Thermal coefficient of expansion (25-1000°C)	7.9 - 8.8	K$^{-1}\times 10^{-6}$
Heat of Fusion	108.86	(J/Kg.mol) $\times 10^{-6}$
Melting Point	2053	K
Boiling Point	3253	K

3.3.2 Mechanical Properties

Typically, alumina is well known of its high hardness which ranges up to 9 Moh scale. Thus, it can be applied for many applications that require a high extent of wear and abrasion resistance such as grinding materials. However, alumina exhibits its design limitations due to its intrinsic stiff and brittle characteristics. For instance, the low flexural strength of alumina, which is a mechanical parameter that is associated with brittleness, makes it unable to resist deformation under load over an extended period of time (Riedel and Chen, 2000).

In addition, the strength of alumina strongly depends on the types of acting forces or stresses as a result of low fracture toughness and the presence of imperfections. As similar to other ceramic-based materials, alumina has higher degree of compressive strength, which is 3790 MPa; however, it is relatively brittle under tensile and bending stresses. By comparison, alumina demonstrates a low fracture toughness of 4.0 $MPa.m^{1/2}$, which is much poorer than that of its counterpart, zirconia, which has 9.0 $MPa.m^{1/2}$ (Lide, 2004). Meanwhile, the Young's Modulus of alumina varies from 330 to 400 GPa, which is comparatively higher if compared to that of cobalt chromium, which is 220 GPa. Similarly, cyclical mechanism such as fatigue and creep can substantially reduce the service lifetime of alumina as well as its resistance to external loading. Under fatigue loading, the stress sustainability of alumina relies on the exposed environment, its manufacturability and the number of cycles (Auerkari, 1996). Other mechanical properties and their values are shown in Table 3.3

Table 3.3: Mechanical Properties of Aluminium Oxide (99 - 99.9 wt%)
(Riedel and Chen, 2000).

Mechanical Properties	Value	Unit
Hardness	15-16	GPa
Flexural Strength	550	MPa
Tensile Strength	310	MPa
Compressive Strength	3790	MPa
Fracture Toughness	4.0	$MPa.m^{1/2}$
Modulus of Elasticity	330-400	GPa
Poisson's Ratio	0.26	-

3.3.3   Chemical Properties

The exceptional chemical resistance of alumina makes it inert to various reactive compounds. For example, alumina is insoluble in inorganic acids and alkali at room temperature but it dissolves slowly in molten salts and oxides at elevated temperature which is greater than 1000°C. Besides, alumina is unaffected by the atmospheric exposure and marine exposure; thus, it resists corrosion that could be formed by chemical reaction between the oxygen and moisture. Furthermore, alumina powders are not hazardous if compared to beryllia or simply beryllium oxide in powder form which is toxic for inhalation and ingestion (Martin, 2007).

3.4   Applications

Nowadays, alumina is widely used in the engineering applications due to its desired combination of properties in physical, mechanical and electrical aspects such as good strength and wear resistance, thermal and electrical insulation, excellent thermal stability and inertness to chemical reaction. Meanwhile, the ease of processing and excess availability makes it extensively employed in the industrial usages (Auerkari, 1996).

Typically, the applications of alumina in industry are based on the grades of alumina in which it is produced. Grades of alumina are determined by the amount of Al_2O_3 content in the alumina matrix, which includes the amount of impurities and other alloying agents that were purposely added for specific industrial usages. Auerkari (1996) has classified the grades of alumina into two categories, which are high-alumina engineering ceramics with at least 99% of Al_2O_3 content and engineering alumina ceramics which owns between 80% to 99% of Al_2O_3 content. For instance, high-alumina engineering ceramics are suitable to be used in structural engineering, street lamps, machine tools, refractories and microwave components while engineering alumina ceramics can be applied on insulators, wear resistant parts, mechanical and electrical appliances (Auerkari,1996).

By viewing the applications of alumina from its properties, the chemical resistivity and translucency make alumina applicable in the envelope of sodium vapour discharge lamps. Meanwhile, owing to its high hardness and low specific heat, refractories bricks and abrasives have accounted for the major markets for alumina–based materials. Besides, alumina is known as the prime materials for spark plugs insulators and furnace linings due to its electrical and thermal insulative characters. From medical point of view, alumina is a suitable material for hip prostheses, which is attributed for its excellent wear resistance that results in a longer service time. Other applications of alumina include sliding gates valves, computer substrates, grinding media and fibre insulation (Carter and Norton, 2007).

Figure 3.4: Applications of Alumina: Hip Prosthesis, Bricks, Spark Plug, Sodium Vapour Discharge Bulb, Sliding Gates Valve (Clockwise)

3.5   Powder Consolidation Methods

Basically, consolidation is a process that involves the application of pressure to compact the fine particles or powdered mass into the desired contour (Callister, 2007). The objective of powder consolidation is to attain densification of green body with minimal microstructural coarsening or transformations (Koch, 2002). This process is essential because the green density formed may impose a significant

influence on the final microstructure properties. The three fundamental powder coalescing methods are uniaxial pressing, isostastic pressing and hot pressing.

3.5.1   Uniaxial Pressing

Uniaxial pressing can be regarded as the consolidation approach that involves the application of pressure in a single direction to transform the powders into a coherent compact within a metal die. Upon completion, the green compact formed will follow the configuration of the die or the flat disc where the pressure is exerted (Callister, 2007). Uniaxial pressing is cost effective due to its ability to produce green body with close dimensional tolerance without the need of high cost (Segal, 1989). The production rates by using uniaxial pressing are relatively high due to the ease of procedure that saves a lot of processing time (Olevsky et al., 2009).

However, uniaxial pressing is difficult to form the intricate geometry of the green samples because the powders do not flow uniformly in the direction perpendicular to the applied pressure. Likewise, the shape of the powder compact is inflexible since it is confined by the rigid die contour upon application of uniaxial pressing. Moreover, density variation is commonly found in the compact after the uniaxial pressing, which may influence the effect of sintering in later stage (Groover, 2010).
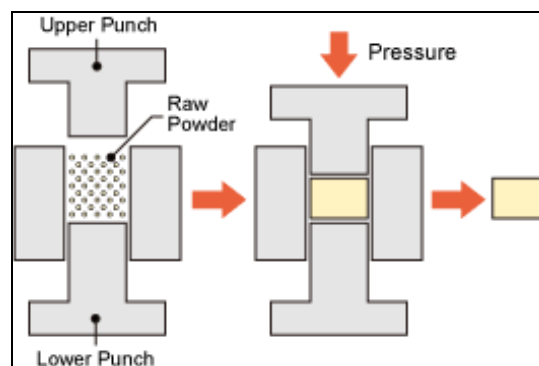
Figure 3.5: Uniaxial Pressing Process (Kyocera, 2010).

3.5.2   Isostatic Pressing

The inadequacies that found in uniaxial pressing has led to the emergence of isostatic pressing. By definition, isostatic pressing is a powder consolidation method which applies uniform pressure from all directions against the powder enclosed in the flexible mold. For that, the term " Isostatic" is used to imply the pressures applied from all directions are equal in magnitude (Groover, 2010). During the process, the pressure is transmitted through the liquid medium such as water or oil in the pressure vessel. Due to the flexible characteristic, the mold will then deform to compact the powder and recover to its initial form after the pressurization is completed (Segal, 1989).

The presence of isostatic pressing has exhibited a wide range of advantages over other powder consolidation techniques. Overall, isostatic pressing can achieve a better densification and smaller grain sizes of green body that yields a nearly zero porosity if compared to that of the samples produced by uniaxial pressing owing to its consistent pressure allocation. Similarly, complicated shapes of green samples are attainable because the pressure is applied uniformly in all directions without the intervention of die wall friction and geometry constraints imposed by hard tooling (Diane, 1993).

Even so, the capital expenditure in isostatic pressing equipment is costly and time consuming due to the complex processing procedures of each specimen. Besides, poor dimensional accuracy of green samples is often attained by isostatic pressing due to the use of flexible mold. Therefore, additional finishing operations is necessary before and after sintering (Groover, 2010). Furthermore, isostatic pressing can be categorized into two alternative forms, which are hot isostatic pressing and cold isostatic pressing.

Hot isostatic pressing (HIP) is a method that employs inert gas as a medium to compress the powder under high pressure and temperature which is higher than the recrystallization temperature of the powder materials. Typically, argon is widely used as the pressure medium due to it inertness and stability in the environment (Koizumi et al., 1991).

With regard to the advantages, HIP process can yield a high green density which ranges between 85% and 95% of theoretical density at low temperature and preserve fine and homogeneous microstructure (Zavaliangos et al., 2001). Despite of the fine grain dense articles, HIP process also forms powder compact with excellent mechanical strength and near final shape parts with minimum machining (Goldman, 2005). However, the HIP process often faces difficulties in in desorbing gases from the powder particle surfaces (Wang, 1976). Meanwhile, the costly and complex processing associated with the HIP process restricts its usages to high cost applications as in the aerospace industry.

Meanwhile, cold isostatic pressing (CIP) is a technique that involves pressure medium such as water or oil to exert uniform hydrostatic pressure against the mold for powder compaction. The term "Cold" is referred to as the isostatic pressing is performed in room temperature, which is dissimilar to the HIP process that is implemented at elevated temperature. Unlike the hot pressing methods, CIP process utilizes rubber or other elastomer materials to fabricate the mold in an oversized manner for shrinkage compensation (Groover, 2010). Likewise, more uniform density and greater applicability to shorter production runs can be obtained through the CIP process. Moreover, CIP method outshines the other alternative, HIP technique in such a way that it requires less expensive tooling during the entire process (Groover, 2010).
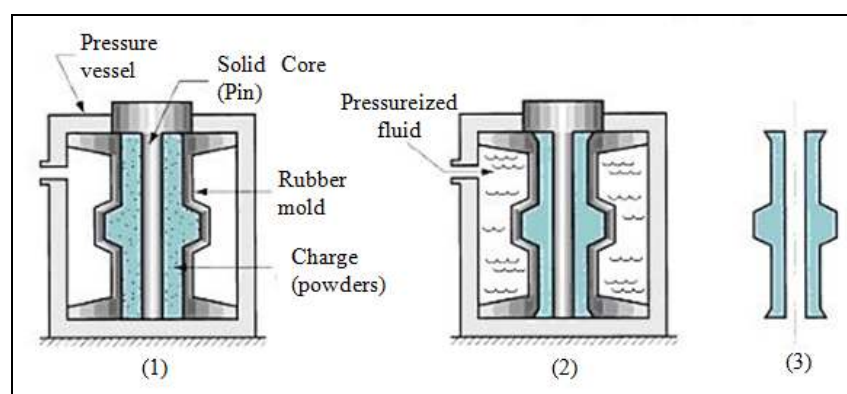
Figure 3.6: Cold Isostatic Process (1)Placement of powder in the flexible mold; (2) Application of hydrostatic pressure against the mold for powder compaction; (3) Pressure is reduced and part is removed (Groover, 2010).

3.5.3   Hot Pressing

Hot pressing, which is also called as hot uniaxial pressing, engages simultaneous application of pressure and heat treatment during sintering. In other words, the powder aggregate is subjected to compaction at a elevated temperature. Commonly, the die used for hot pressing process is made of refractory materials such as graphite to withstand extreme temperature and exertion of pressure in a concurrent manner (Segal, 1989). As a result, no subsequent sintering is required after the hot pressing process.

Unlike uniaxial pressing, hot pressing is able to produce a green compact with higher density without appreciable grain growth at relatively low temperatures. However, both hot pressing and uniaxial pressing are similar in such a way that their process are suitable for the fabrication of flat plates, block and cylinders whose fabrications require less complicated geometry (Segal, 1989).

In contrast, hot pressing is inappropriate to be used for powder consolidation if overall process time is the priority. For instance, hot pressing is time consuming because both heating and cooling process of die and mold are necessary to be carried out for each cycle of hot pressing process. In addition, the hot pressing mold usually has a short service lifetime, despite of its expensive fabricating cost (Callister, 2007). Also, the performance of hot pressing is frequently limited by the low strength of graphite die and the simple article shapes (Segal, 1989).
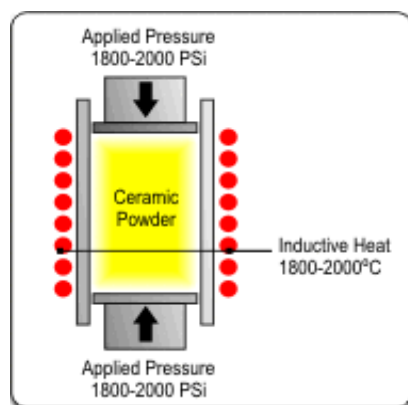
Figure 3.7: Hot Pressing Process (A to Z of Materials [AZOM], 2010).

3.6   Sintering Methods

Sintering can be defined as the heating phenomenon which converts compacted powders into a body with desired properties at temperature below the melting point of the materials via the formation of bonding between particles (Hosokawa, 2007). Several factors such as particle size, green density, firing schedule and other important considerations should be highlighted in the sintering kinetics of alumina or other ceramic-based materials due to their impact on the final microstructure characteristics (Smothers and Reynolds, 1954).

3.6.1   Pressureless Sintering

As the name implies, pressureless sintering coalesces powders into a sintered body without the assistance of pressure throughout the entire heating process. It can be categorized into two types, which are conventional sintering and two step sintering. Pressureless sintering is well recognized by the industry due to its inexpensive cost and minimal energy usage without compromising the quality of the material considerably if compared to other methodologies.

Conventional sintering, which sometimes referred to as single step sintering (SSS), engages constant heating rate cycle with a dwell time at certain sintering temperature. In conventional sintering, the material is first heated at its surface before the heat flows inward to the inner part of the materials. In performance aspect, conventional sintering can produce a sintered body with acceptable densification and moderate grain growth (Maca et al., 2009).

However, the heat condution that flows from the exterior surface to interior side of the compacted powder creates an undesirable temperature gradient and result in higher temperature obtained at the sample surface than its core. Therefore, the uneven heat distribution of conventional sintering will deteriorate the final microstructure of the sintered body volumetrically. Besides, the increase in process time associated with the conventional sintering will lead to the grain coarsening as a

result of a slower heating rate and isothermal sintering. Likewise, high heating rates would cause thermal gradient within the samples and lead to compact distortion and inhomogeneous microstructure (Oghbaei et al., 2010).
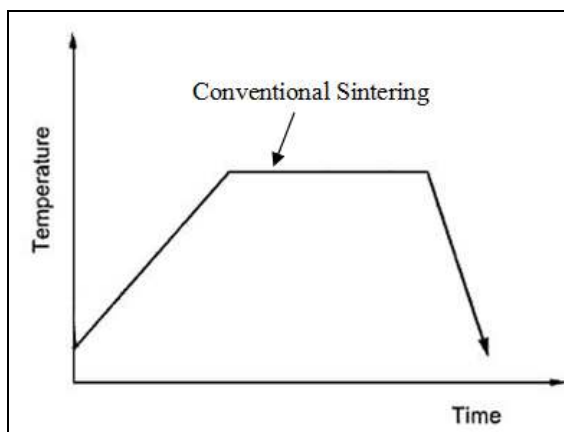
Figure 3.8: Schematic Showing The Thermal Cycle of Conventional Sintering (Kang, 2005).

In general, two-step sintering (TSS) can be classified into two patterns which have their respective unique temperature profiles. As shown in Figure 2.6, the first regime of TSS maintains the heating of samples at relatively low temperature at first stage to allow the surface diffusion to predominate in the microstructure before increasing the temperature to higher level at the second stage of sintering for densification purpose.

Meanwhile, the temperature profile for second pattern of TSS follows the path where the sintering is first applied to the samples at constant heating rate (CHR) until a high temperature to induce pre-coarsening and attain initial high density. Without maintaining at that high temperature, the sample is then cooled down rapidly by about 100°C and held at a lower temperature by second stage sintering for a extended period to enhance the densification without the occurencce of apparent grain growth and surface diffusion (Wang et al., 2009).

For second pattern of TSS, Chen et al. (2000) have claimed that the elimination of the supercritical pores can be achieved during the first stage sintering while the unstable behaviour of the remaining pores can ease the second stage

sintering at a lower temperature without experiencing further grain growth. Therefore, this TSS regime produces a body with finer grains and higher density than those obtained by using the SSS approach.

TSS methods exhibit a wide range of advantages over other sintering techniques. The optimum TSS regime led to a remarkable reduction in grain size by suppressing the accelerated grain growth of alumina powders to about 500nm, which is much smaller than the 1 to 2μm of grain size achieved by SSS approach (Hesabi et al., 2009). Besides, growth ratio, which is the ratio of final grain size to initial particle size, can be decreased effectively through the application of two-step sintering with the appropriate temperatures (Wang et al., 2009).
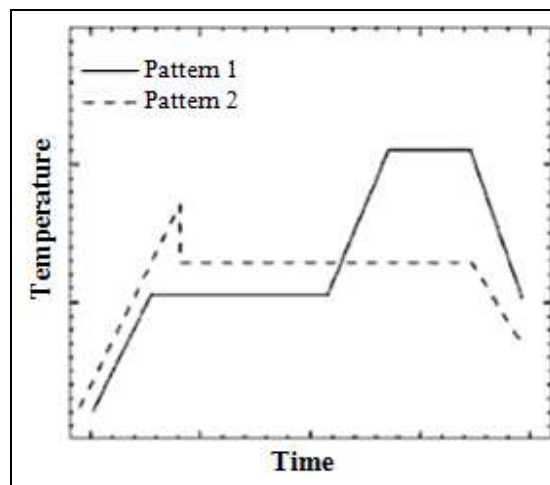
Figure 3.9: Temperature ramping profile for two-step sintering (Hosokawa, 2007).

3.6.2 Spark Plasma Sintering

Spark plasma sintering (SPS), which is also known as as pulse electric current sintering, field-assisted sintering technique or plasma activated sintering, is an approach of refining ceramics properties through rapid sintering. The sintering mechanism is initated by the application of pulsed DC current which directly heats up the electrically conductive die uniformly from all direction and transfer the heat to the specimens that undergo hot uniaxial pressing previously for densification purpose (Salamon and Shen, 2007).

The emergence of SPS processing has exhibited numerous advantages over other atmospheric sintering methods. Firstly, SPS is efficient whereby it enhances the densification rates at a relatively low sintering temperatures that yields the reduction in energy consumption and sintering time. Owing to its rapid heating rate and low firing temperature, SPS is able to increase the densification and suppressing grain growth at a greater extent (Bansal and Singh, 2009). Besides, the nature of pulsed electric current in SPS approach can effectively affect the defect migration, crystal growth, phase transformation and diffusion of the materials (Guo and Tuan, 2004).

Despite of the specific advantages, SPS process seldom produces a sintered body with homogeneous microstructure. Another limitation of SPS is that undesirable by-products such as the vapor deposit can be produced after the application of SPS process (Guo et al., 2004). Moreover, SPS process tends to enhance grain growth if the heating rate, sintering temperature, and dwell time are not precisely selected. Meanwhile, the industrial applications of the SPS process is constrained due to its restricted shape capability (Basu et al., 2004).
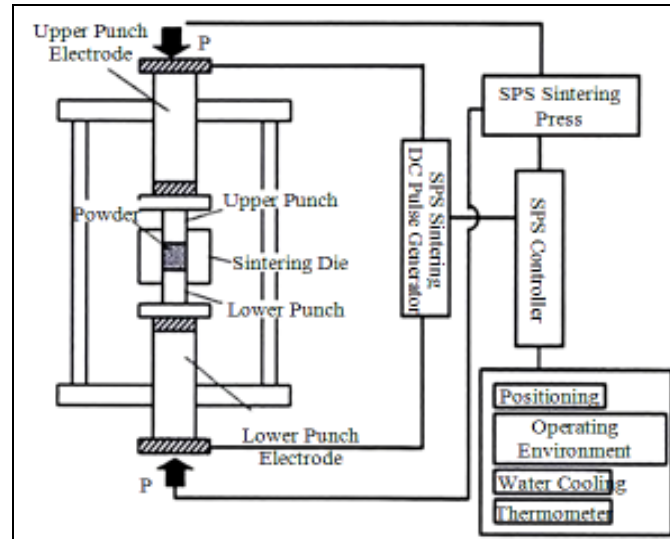
Figure 3.10: Spark Plasma Sintering System Configuration (Aalund, 2009).

3.6.3 Microwave Sintering

Microwave sintering utilizes electromagnetic waves to generate heat within the material before transforming the heat to the entire material volumetrically in a non contact manner (Yadoji et al., 2003). The extensive use of microwave sintering is attributed to its uniform heat distribution that yields a higher densification, which is much better than those density achieved by the pressureless sintering that troubled by the formation of agglomerate during the pre-sintering stage (Biamino et al., 2006). Microwave sintering can produce a finer grain size than those produced by pressureless sintering due to its short sintering period that inhibits further grain growth. Microwave sintering also overwhelms pressure-assisted sintering by not having the disadvantage of limited shape capability (Souto et al., 2007). Besides, this technique is good at energy saving because the heat produced are self generated while rapid temperature rise and drop can be achieved by the selective heating operation of microwave sintering (Ohji et al., 2009).

Occasionally, imhomogeneity of sintered materials might result in the microwave sintering due to some intrinsic problems. Thus, the employment of microwave hybrid heating (MHH) technique is used to preserve a microstructural refinement of the sintered materials by introducing direct microwave heating and infrared as the heat source. Moreover, ceramic materials subjected to microwave sintering are susceptible to local thermal runaway, melting or cracking during rapid heating because the microwave absorption coefficient in many ceramics augments exponentially with the temperature (Bengisu, 2001).
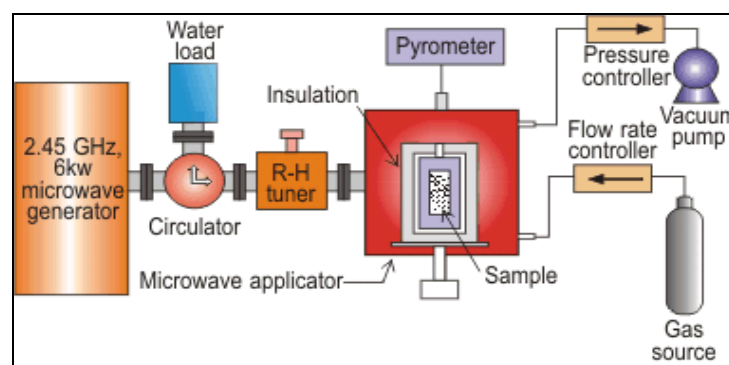
Figure 3.11: Microwave Sintering Process (AZOM, 2010).

3.7 Effects of Various Additives on the Properties of Alumina

3.7.1 Niobium Oxide

According to the research of Hsu (2005), the addition of Niobium Oxide, Nb_2O_5 in alumina effectively enhances the densification rate at a lower sintering temperature and shorter sintering period. High purity θ-Al_2O_3 powder with average particle size of 0.21μm was used as the starting powder whilst various amounts of high purity Nb_2O_5 powder ranged from 0.5 to 2.0 mol% were used as the additives. The mixture was subjected to uniaxial pressing at 115 MPa and followed by sintering between 1300°C and 1550°C at a heating rate of 10°C/min and various holding time.

As shown in Figure 3.12, the density and the average grain size of alumina increase with the sintering temperature and period for all samples. For instance, over 95% of the theoretical density of Nb_2O_5 doped samples could be obtained at 1350°C after 2 hours of sintering. At this point, the sintering temperature of doped alumina is lowered than that of the pure alumina for 100 to 150°C. Nevertheless, the doping of Nb_2O_5 could promote the grain growth. For instance, Nb_2O_5 doped alumina exhibited a larger grain size than that of the pure alumina at the same sintering time. However, the pinning effect of secondary phase aluminium niobate, $AlNbO_4$ formed in 0.5 to 2.0 mol% Nb_2O_5 doped sample decreases its grain sizes between 1350°C and 1550°C by retarding the grain boundary mobility (Hsu, 2005).
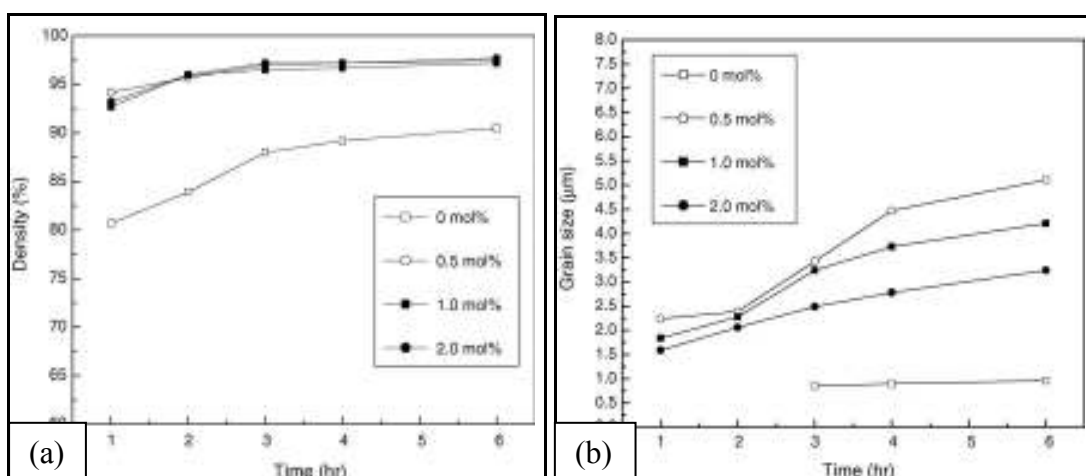
Figure 3.12: Variation of (a) Density (b) Grain Size As A Function of Holding Time At 1350°C (Hsu, 2005).

3.7.2   Manganese Oxide

Based on the research of Sathiyakumar et al. (2001), the addition of manganese oxide, MnO, could produce a relatively uniform microstructure with high density at elevated temperature while the presence of pores is unavoidable. In this experiment, 0.1 to 3.0 wt% composition of MnO were added into the starting material, the sol gel derived alumina powder. The mixture was compressed by using uniaxial pressing and subsequently sintered between 1400°C and 1600°C. The results shown that 98 to 99% of theoretical density (T.D) can be attained by the 0.1 wt.% MnO doped alumina when sintered at 1550°C for 3 hours, which is analogous to 98.5% of T.D yielded by pure alumina under the same condition. Thus, high sintering temperature is needed for the addition of MnO to enhance the densification to a greater extent.

At the same time, inhomogeneous grain growth, where finer grains were surrounded by larger grains, was produced by the doped samples if compared to the homogeneous grain growth yielded by pure alumina with some isolated pores. Significant grain growth with grain size between 20 and 100μm and the presence of intergranular and intragranular pores were observed when MnO content is increased up to 0.5 wt.%. Slight decrement in the hardness was occurred as the amount of MnO was increased up to 0.5 wt.%. However, further increase of MnO concentration improves the hardness. For example, the maximum hardness, 23 GPa, was reached by alumina with 3.0 wt.% of MnO at 1550°C due to the formation of secondary intergranular phase in the form of continuous layers (Sathiyakumar et al., 2001).

(a)   (b)
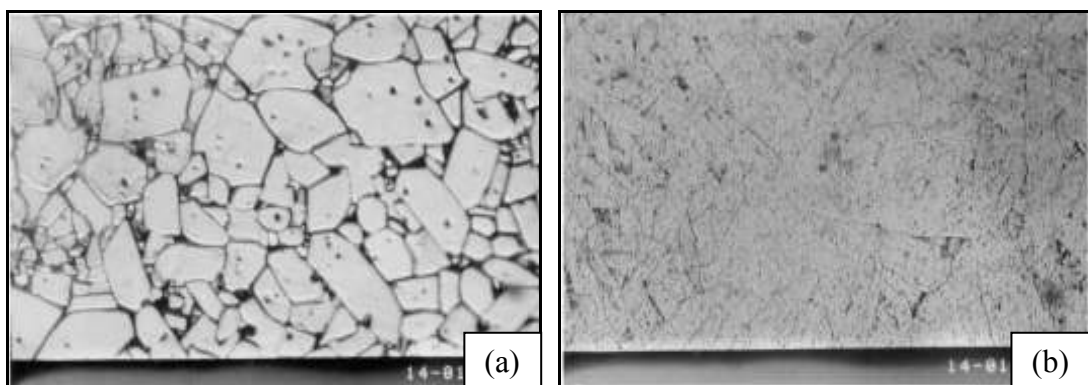
Figure 3.13: Micrograph of Alumina Sintered At 1500°C, (a) Pure (b) 0.5 wt.%
Manganese Oxide (Sathiyakumar et al., 2001).

3.7.3   Zirconium Oxide

Wang et al. (2009) has analyzed the densification and grain growth of fine alumina-zirconia ceramics by using two-step sintering. The experiment was started by uniaxially pressing the as received α-Al_2O_3 powder of 150 nm average particle size with 5 wt% of zirconium oxide or zirconia, ZrO_2 at 150MPa and followed by two step sintering. The first step sintering temperature was ranging between 1400 and 1450°C at heating rate of 10°C/min while the second step isothermal sintering temperature was lowered to between 1300 and 1400°C with cooling rate of 30°C/min.

Zirconia could induce a pinning effect that effectively reduces the degree of grain growth in alumina by allowing a higher second step sintering temperature to be used to enhance the densification while preserving small grain size (Bodišová et al., 2007). For example, smaller grain sizes of zirconia doped alumina from 0.47 to 0.62 μm could be observed at 1350°C if compared to 0.38 to 0.90 μm of grain size achieved by pure alumina sintered at 1150°C. This is owing to the locations of fine zirconia grain at grain boundaries or triple junction of alumina that inhibits grain from expanding under elevated temperature (Wang et al., 2009). However, over 99 % of T.D attained by alumina-zirconia sample was largely attributed to the application of two-step sintering rather than the presence of zirconia. Similar results was obtained in the research of Menezesa et al. (2008) which stated that high densification is greatly contributed by the effect of microwave sintering regardless of the composition of zirconia in alumina.
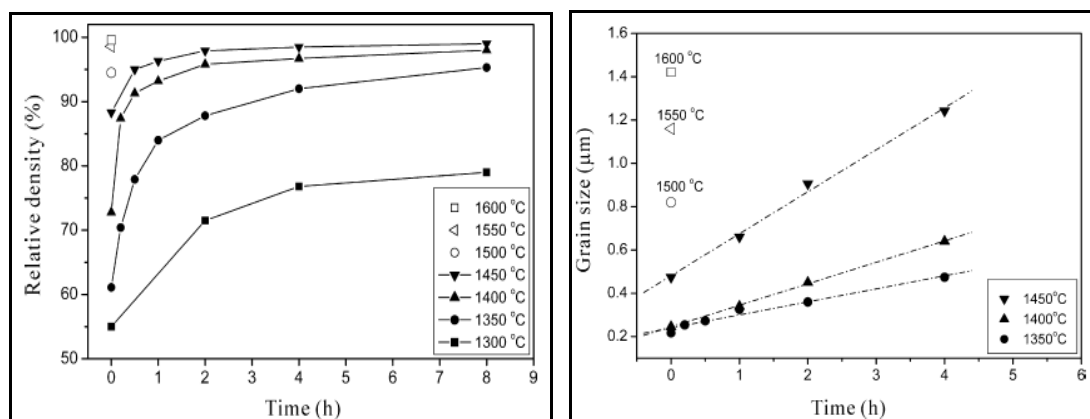
Figure 3.14: (a) Relative Density (b) Grain Size of Alumina Specimens Against Sintering Time At Various Temperatures (Wang et al., 2009).

3.7.4 Magnesium Oxide

The effect of magnesium oxide, MgO on the grain growth and density of alumina was examined in the research of Bae et al. (1994). The starting material is ultrapure α-Al_2O_3 whilst CaO and MgO serve as the additives. The mixture was compressed cold isostatically at 196.2 MPa and pressureless sintered at 1900°C for 1 hour. The results show that the effects of MgO on the grain growth and densification depends on the presence of impurities in the alumina. For ultrapure alumina, the final grain size increases linearly with the amount of MgO. Unlike the liquid film formed by CaO that triggers the development of abnormal grain growth, the inhibitive nature of MgO in the presence of impurities is due to the formation of amorphous phase that restrains MgO from surpassing its solubility limit at high temperature.

However, this result was dissimilar with previous studies which reported that the addition of MgO can reduce the grain boundary mobility by using 99.99% purity of commercial alumina powder (Marucus et al., 1972). This is because the alumina with such purity is still likely to be impure if compared to the ultrapure alumina that is free of contamination. MgO also helps to promote the densification kinetics during pressureless sintering. For example, 96% of relative density can be achieved by 200 ppm of concentration of MgO while CaO of the same composition can only attain less than 91 % of relative density (Bae et al., 1994).
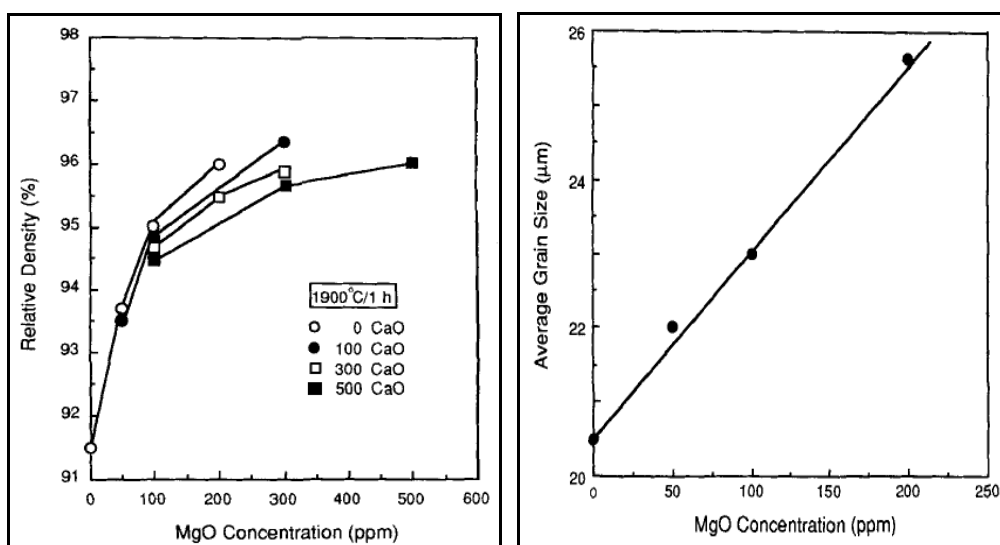
Figure 3.15: (a) Relative Density (b) Average Grain Size As A Function of MgO Concentration 1900°C For 1 Hour (Bae et al., 1994).

3.7.5   Titanium Oxide

Due to the limitations of the previous additives, the introduction of titanium oxide, or titania, TiO_2 is believed to have a further refinement on the sintering kinetics, grain size and the mechanical properties of alumina. For that, Sathiyakumar et al. (2001) has analyzed the influence of TiO_2 additive on density, microstructure and mechanical properties of alumina. In this experiment, the starting material was sol-gel derived alumina whereas various compositions of titanium oxide, ranging from 0 to 4 wt% were used as the dopants. The well dispersed mixture was first uniaxially pressed and subsequently sintered at temperatures from 1400 to 1600°C for 3 hours.

According to the research of Wang et al. (2008), TiO_2 is a beneficial additive which is capable of yielding a higher sintered density at a lower sintering temperature. For instance, the density of alumina with 0.2 wt.% concentration of TiO_2 increases from 81 to 98% of T.D when the material was sintered at a lower sintering temperature of 1400°C. Nevertheless, only 96% of T.D could be obtained for pure alumina despite of sintering at a elevated temperature of 1500°C. Conversely, alumina with 0.1 wt.% amount of TiO_2 is sufficient to achieve 98% of T.D at 1500°C while further increase in the TiO_2 content will not enhance the density as the sintering temperature increases (Sathiyakumar et al., 2001).
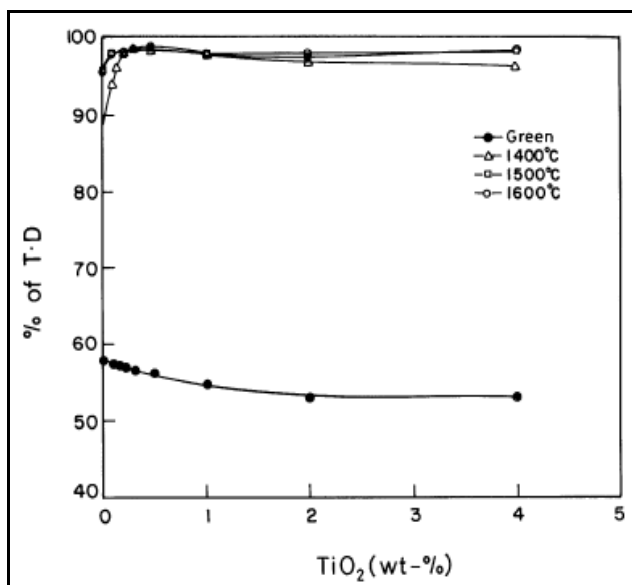
Figure 3.16: (a) The Effect of Sintering Temperature On Sintered Density of TiO_2 doped Al_2O_3 (Sathiyakumar et al., 2001).

Recent studies by Chen et al. (2009) had further verified Sathiyakumar et al. results by revealing that less than 0.3 wt.% of TiO_2 can effectively quicken the densification rates of alumina and cause the sample to achieve about 95% of T.D. After that, the accelerating trend in density increment slow down with further increase in TiO_2 content up to 0.45 wt.%. Beyond this value, almost no noticeable increment in bulk density of the samples could be observed.

Usually, the addition of TiO_2 content in alumina accelerates the grain growth. This is evidenced when the grain size enlarges as the TiO_2 content increases from 0 to 0.2 wt.%. However, grain growth was decreased when TiO_2 content increases beyond its solubility limit from 2.0 wt.% to 4.0 wt.%. This is due to the formation of secondary phase, aluminium titanate, Al_2TiO_5 upon the solubility limit which acts as the pinning effect that inhibit further grain growth (Sathiyakumar et al., 2001). Likewise, the experimental results of Horn et al. (1995) also shown that the grain size expands with increasing TiO_2 content. For instance, after sintering for 16 hours at 1300°C, the grain size of the alumina with 0.4 wt.% of TiO_2 increases to 0.78 μm, which is considered as normal grain growth if compared to the undoped sample that reached grain size of 0.6 μm under same condition. Interestingly, about 25 to 60% of volume fraction of anisotropic grains were transformed from normal grains for TiO_2 samples, ranging from 0.15 to 0.40 wt.% when the temperature is raised to 1400 and 1450°C. These anistrophic grains have reduced grain growth by inducing impingement of the large anisotropic grains and the loss of grain boundary area into the fine grain size matrix (Horn et al., 1995).
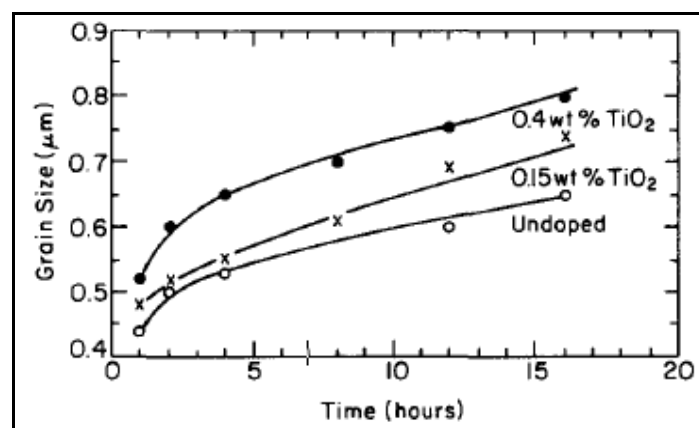
Figure 3.17: Variation of Grain Growth of Undoped And TiO₂-Doped Alumina At 1300 °C (Horn et al., 1995).

Nonetheless, further increase in TiO_2 content in alumina with extended sintering time results in adverse effect on the grain size. For example, alumina doped with 0.6 wt.% TiO_2 encountered abnormal grain growth, which is about 2.4 μm after it was sintered for 1 hour. Eventually, the grain size expands considerably to 13 μm after sintering for 16 hours at 1300°C. Thus, 0.4 wt.% or less concentration of TiO_2 in alumina is adequate to prevent excessive grain growth at low sintering temperature, which is below 1350°C for short sintering period (Horn et al., 1995).

Noteworthily, the increase of TiO_2 content in alumina contributes to a greater flexural strength. For instance, a flexural strength of 315 MPa was recorded for pure alumina sintered at 1600°C but, under the same sintering temperature, the flexural strength surged to 353 MPa when the amount of TiO_2 was increased to 0.1 wt.%. Afterward, further increase in TiO_2 content reduces the flexural strength gradually until it reaches 347 MPa at 4.0 wt.% of TiO_2. Noticeably, the maximum value of flexural strength, which is 409 MPa, could be attained by alumina with TiO_2 content of 0.2 wt.% sintered at 1400°C (Sathiyakumar et al., 2001).
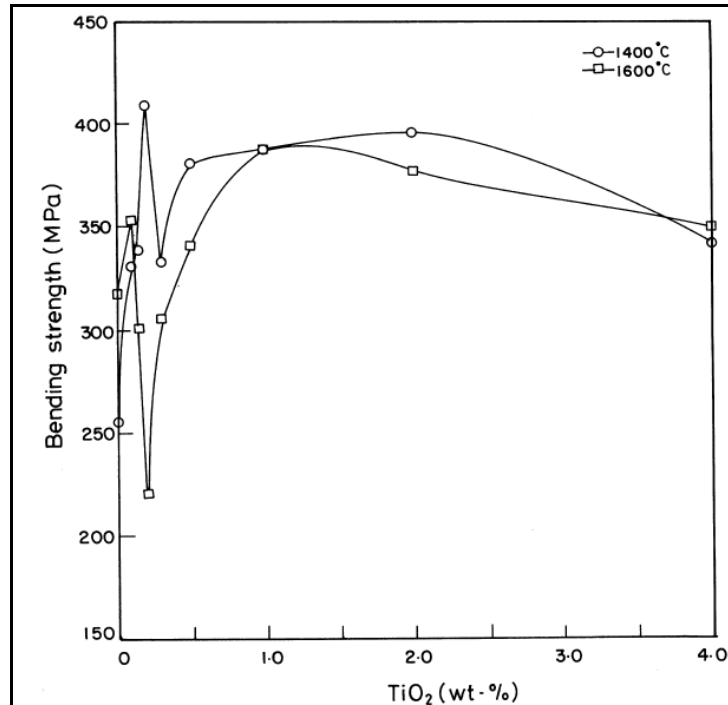
Figure 3.18: Flexural Strength of TiO_2 doped Al_2O_3 (Sathiyakumar et al., 2001).

CHAPTER 4

METHODOLOGY

4.1   Introduction

In this chapter, standard experimental apparatus and techniques that were used continually throughout the entire research will be covered in details. Besides, experiment procedures with regard to the alumina research such as powder and green body preparation, sintering, finishing as well as measurement processes will be discussed specifically with table and diagram for enhanced clarification.

4.2   Powder Preparation

In this experiment, the as received commercially available materials 99.8% pure alumina (NanoAmor, USA) and 99.9% pure titanium oxide (TiO_2) powder (NanoAmor, USA) were used as the starting powders. The chemical analysis and properties of these powders are provided in Table 4.1 and Table 4.2. Five different compositions of TiO_2 powder, ranging from 0, 0.5, 1.5, 3.0 and 5.0 wt%, were added into the alumina powder through a process involving ultrasonification and ball milling.

Both starting powders, TiO_2 and Al_2O_3 were measured according to the composition required and poured into a beaker containing approximately 200 mls of ethanol. The solution was then subjected to ultrasonic pulses at $28 - 34$ kHz for half

an hour to improve the dispersion and homogeneity of TiO_2 in the alumina powder. The mixture was then poured into a high density polyethelene (HDPE) bottle followed by zirconia balls as the milling media. The mixture was subsequently ball-milled for at least 1 hour. Sieve was used to separate the milling balls from the slurry. Next, the slurry was dried by the oven for overnight at 60°C to remove ethanol through evaporation process. Afterward, the dried cake was crushed and sieved through a 212 μm mesh stainless steel sieve to obtain ready-to-press powders.

Table 4.1: Characteristic of the starting Al_2O_3 powder

Chemical composition	Al_2O_3	Unit
Aluminium dioxide (Al_2O_3)	99.50	wt%
Iron oxide (Fe_2O_3)	0.30	wt%
Magnesium oxide (MgO)	0.001	wt%
Silicon dioxide (SiO_2)	0.05	wt%
Mean particle size	27.0	nm
Theoretical density	3.98	g/cm^3

Table 4.2: Characteristic of the doping TiO_2 powder.

Chemical composition	TiO_2	Unit
Titanium oxide (TiO_2)	99.0	%
Barium (Ba)	0.0002	%
Calcium (Ca)	0.01	%
Cadmium (Cd)	0.0003	%
Niobium (Nb)	0.07	%
Phosphorous (P)	0.27	%
Plumbum (Pb)	0.006	%
Strortium (Sr)	0.0002	%
Zirconium (Zr)	0.019	%
Mean particle size	5.0	nm
Theoretical density	3.9	g/cm^3

4.3 Green Body Preparation

Both undoped and TiO_2-doped alumina powders were firstly compacted by uniaxial pressing at about 2.5 MPa into disc (20 mm dia. x 5 mm thickness) and rectangular bars (32 x 13 x 6) mm, respectively. For each powder composition, one disc (each weighing 2.5 g) and one bar (weighing 2.5 g) were fabricated. Then, the green compacts were marked using the sample identification codes shown in Table 4.3. Subsequently, the samples were again compressed by cold isostatic pressing (CIP) at 200 MPa to ensure homogeneous compaction and to induce uniform shrinkage that yields an improved densification.

Table 4.3: Sample identification codes employed in present study.

TiO_2 (wt%)	Sintering Temperature (°C)		
	1250	1350	1450
0	A1	A2	A3
0.5	F1	F2	F3
1.5	G1	G2	G3
3.0	H1	H2	H3
5.0	I1	I2	I3

4.4 Sintering

The green samples were subjected to pressureless sintering under the ambient condition, using a standard rapid heating furnace at various sintering temperature ranging from 1250°C to 1450°C. Sintering profile of 10°C/min. ramp rate and 2 hours soaking time were employed for all samples.

4.5   Grinding and Polishing

The sintered disc samples were firstly ground by various grade of SiC papers range from 120, 240, 600, 800 and 1200 successively. Polishing was performed with 6 μm and 1 μm diamond paste on the samples to achieve a fine surface finish prior to Vickers hardness testing, XRD and SEM evaluation.

4.6   Bulk Density Measurement

The bulk densities of dense compacts (low porosity) were measured by employing the water immersion technique based on the Archimedes principle. Distilled water was used as the immersion medium in this measurement.

However, special attention was required when measuring the low density samples (high porosity) in the water. Measurement could be taken when the reading from the balance is constant, where all the pores had been penetrated by water completely. The excess weight of the water in the pore was taken out from the calculation to prevent from overestimating the value of the sample's density. The relative density was calculated by taking the theoretical density of alumina as 3.98 Mgm^{-3}. The bulk density (ρ) of the samples was calculated using equation (4.1).

$$\rho = \frac{W_a}{W_a - W_w} \rho_w \qquad (4.1)$$

Where

ρ = Bulk density of the sample

W_a = Weight of the sample in air

W_w = Weight of the sample in water and

ρ_w = Density of the distilled water which varies with temperature.

4.7 Young's Modulus Determination

Sonic resonance technique was used to measure the Young's modulus of the rectangular samples by using a commercial testing instrument. The vibrations were physically induced in the samples by tapping while the resonant frequency of the samples generated was measured by monitoring and evaluating the vibrational harmonics of the samples through the use of a transducer. The Young's modulus is calculated from the measured natural frequency based on the standard test method (ASTM E1876-97). The Young's modulus is computed by using equation (4.2):

$$E = 0.9465\left(\frac{m\,F_f{}^2}{b}\right)\left(\frac{L}{t}\right)^3 T_1 \qquad (4.2)$$

where

E	= Young's Modulus or Modulus of Elasticity (Pa)
m	= Mass of the rectangular bar (g)
b	= Width of the bar (mm)
L	= Length of the bar (mm)
t	= Thickness of the bar (mm)
F_f	= Fundamental resonant frequency of bar in flexure, (Hz)
T_1	= Correction factor for fundamental flexural mode to account for finite thickness of bar, Poisson's ratio etc., calculated using equation (4.3)

$$T_1 = 1 + 6.585\left(1 + 0.0752\mu + 0.8109\mu^2\right)\left(\frac{t}{L}\right)^2$$

$$-0.868\left(\frac{t}{L}\right)^4 - \frac{8.340\left(1 + 0.2023\mu + 2.173\mu^2\right)\left(\frac{t}{L}\right)^4}{1 + 6.338\left(1 + 0.1408\mu + 1.536\mu^2\right)\left(\frac{t}{L}\right)^2} \qquad (4.3)$$

where

μ	= Poisson's ratio which was taken as μ = 0.23 (Munro, 1997).

4.8   **Vickers Hardness Determination**

Vickers Hardness testing method was used to determine the hardness of the sintered alumina samples. The indentations were made by using a pyramidal diamond indenter with an applied load of 0.2 kgf, 0.3 kgf, 0.5 kgf and 1.0 kgf.

During the test, the load was applied gradually, without impact, and held for 10 seconds to create an impression. The physical quality of the indenter and the accuracy of the applied load as defined clearly in ASTM E384-99 and ISO 14705 must be controlled to obtain the correct results. After the removal of the load, the two impression diagonals, D_1 and D_2, as shown in Fig. 4.1, were measured with a filar micrometer built in the attached microscope on the Vickers machine to the nearest 0.1 μm, and then averaged. The Vickers hardness (H_v) is calculated based on the surface area of the indent by using equation (4.4):

$$H_v = \frac{1.854P}{(D)^2} \tag{4.4}$$

where

P   = applied load

D   = average diagonals $= H_v = \dfrac{D_1 + D_2}{2}$
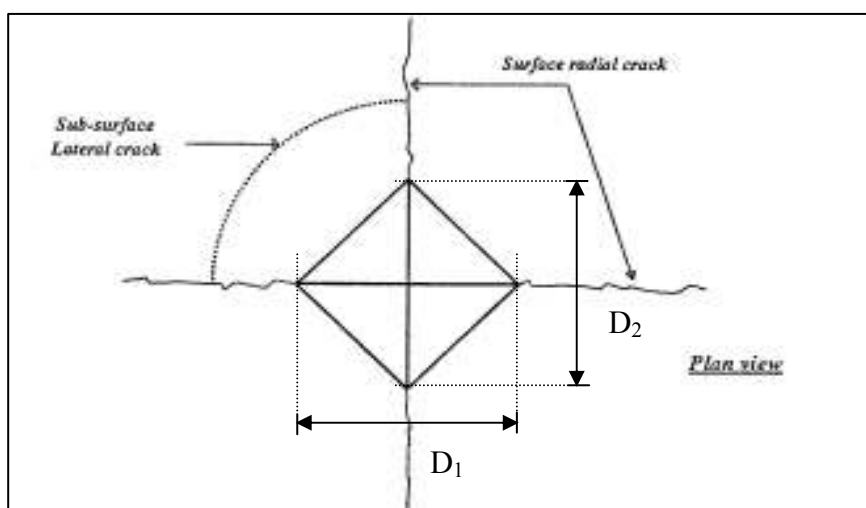
Figure 4.1: Schematic Indentation Fracture Pattern of An Idealized Vicker Palmqvist Crack System.

4.9 Microstructure Examination

The morphology of the starting powders and the microstructural evolution of the sintered samples were examined by using Hitachi scanning electron microscope (SEM). By using SEM, the resolution of the sub-micron dimensional features on the surface of a material and the element composition of the samples were able to be determined. SEM focuses a small spot of electrons on the thick specimen. With electrostatic or electromagnetic force, the samples were scanned in a series of line. Electrons emerging from the upper specimen surface are collected by an electron detector and used to produce an image on a T.V. monitor as a series of lines. Before performing SEM analysis, selected sintered samples were thermally etched at 50°C below the sintering temperature of the sample at a heating and cooling rate of 10°C/min and with a holding time of 30 minutes before cooling. Upon cooling down, the samples were coated with a gold palladium, which is a conductive layer to prevent charging in the microscope so that a clear microstructure, especially the grain boundary can be attained. After obtaining the SEM micrograph, linear interpolation was carried out to determine the average grain size.

4.10 X-Ray Diffraction (XRD)

X-Ray diffraction (XRD) provides information that is pertinent to the crystal lattice of the material and the presence of crystalline phases. Besides, the information on the degree of crystallization and the orientation texture in the material are able to determined from XRD. In the present work, the phases present in the powders and the sintered samples were determined at room temperature by using X-Ray diffraction (Shimadzu XRD-6000, Japan) with Cu-Kα as the radiation source using a scan speed and step scan of 0.5° /min and 0.02° respectively, at 35 kV and 15 mA. The peaks obtained were compared to standard reference JCPDS-ICDD (Joint Committee of Powder Diffraction Standard – International Center for Diffraction Data) files for alumina (No. 10-0173), anatase TiO_2 (No. 21-1272) and rutile TiO_2 (No. 21-1276), aluminium titanate (No. 41-0258).

CHAPTER 5

RESULTS AND DISCUSSIONS

5.1   Density

As shown in Figure 5.1, the addition of TiO_2 has promoted the densification of Al_2O_3 at lower sintering temperature. This could be evidenced by the result of Al_2O_3 containing up to 5.0 wt.% TiO_2, which attained 95% of theoretical density (TD) after 1350°C of sintering while undoped alumina could only achieve 92.29% of TD when it was sintered at a 1450°C. Hence, it was shown that 5.0 wt.% TiO_2 doped alumina could produce a better densification efficiently than the undoped sample even when it was sintered at a temperature which was reduced for 100°C. Besides, all doped samples reached approximately 96% of TD when they were sintered at 1450°C. if compared to 92.29% of TD achieved by pure alumina at this condition. Similar bulk density (~96% of TD) could also be attained by smaller percentage of TiO_2 (0.5 wt%, 1.5 wt.% and 3.0 wt.%) at higher temperature. This improvement can be verified by the research conducted by Wang et al. (2008), which stated that the trend of low sintering temperature becomes more evident as the addition level increases from 0.5 to 4.0 wt.% of TiO_2.

Moreover, Figure 5.2 exhibits an increasing trend for the bulk density of Al_2O_3 when it was doped with various composition of TiO_2 at sintering temperature ranged from 1250°C to 1450°C. Noticeably, the maximum relative density, 96.03%, or 3.822 g/cm^3 of bulk density occurred when alumina is doped with 0.5 wt.% TiO_2 at 1450°C. From the graph, it is observable that higher sintering temperature is more favourable in enhancing the bulk density of alumina. This trend can be supported by

research of Ting et al. (2008) which indicated that bulk density of alumina ceramics increased with sintering temperature ranging from 1250°C to 1500°C for most of the samples containing up to 5.0 wt.% TiO_2 (Ting et al., 2008). However, it was also shown that the addition of TiO_2 amount up to 3.0 wt.% and 5.0 wt% only increased the bulk density insignificantly at 1250°C and 1350°C whilst the relative density at these two compositions stagnate at around 95.8% at 1450°C sintering.
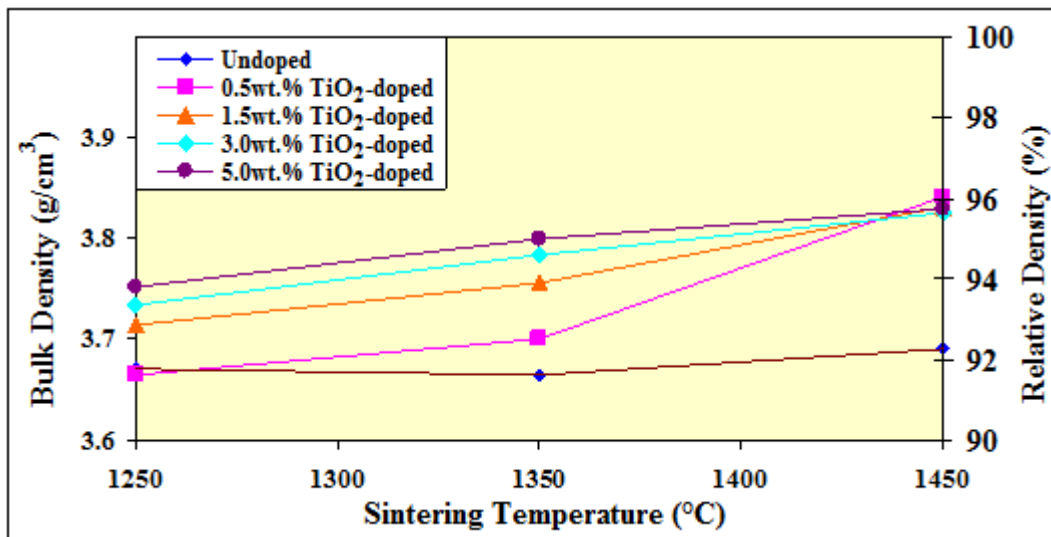
Figure 5.1: Bulk And Relative Density Variation of Al_2O_3 Doped With Different TiO_2 Composition As A Function of Sintering Temperature
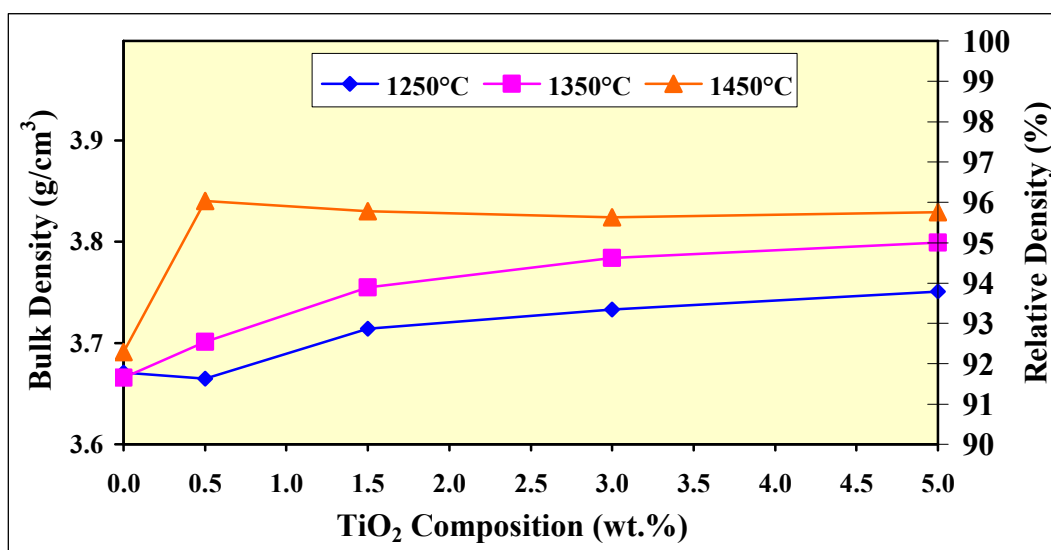
Figure 5.2: Bulk And Relative Density Variation of Al_2O_3 As A Function of TiO_2 Composition At Different Sintering Temperature

The average shrinkage of the TiO_2 doped alumina was plotted against the sintering temperature in Figure 5.3 to determine the relationship between the two parameters. Generally, the resulting shrinkage behaved in an ascending manner when the sintering temperature was increased. In the interim, it seems that the addition of 1.5 wt.% TiO_2 was the shrinkage limit as the samples at all temperature cease to shrink upon this concentration, as exhibited in Figure 5.4. By matching the bulk and relative density variation, it was noted that both of the trends were comparable to those of average shrinkage. Thus, there is a linear relation between the bulk density and percentage of shrinkage. In other words, the sample would be denser due to a smaller size that is equivalent to a greater percentage of shrinkage.
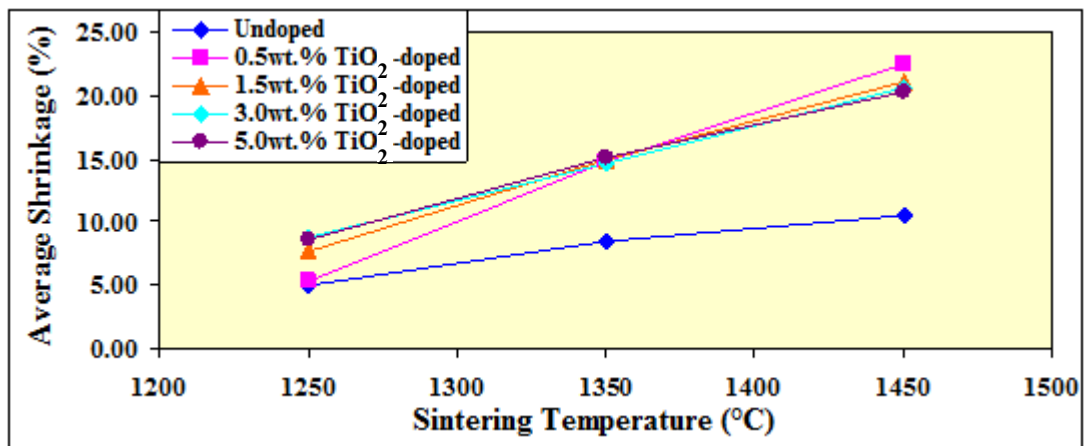
Figure 5.3: Average Shrinkage Variation of Al₂O₃ Doped With Different Amount of TiO₂ As A Function of Sintering Temperature
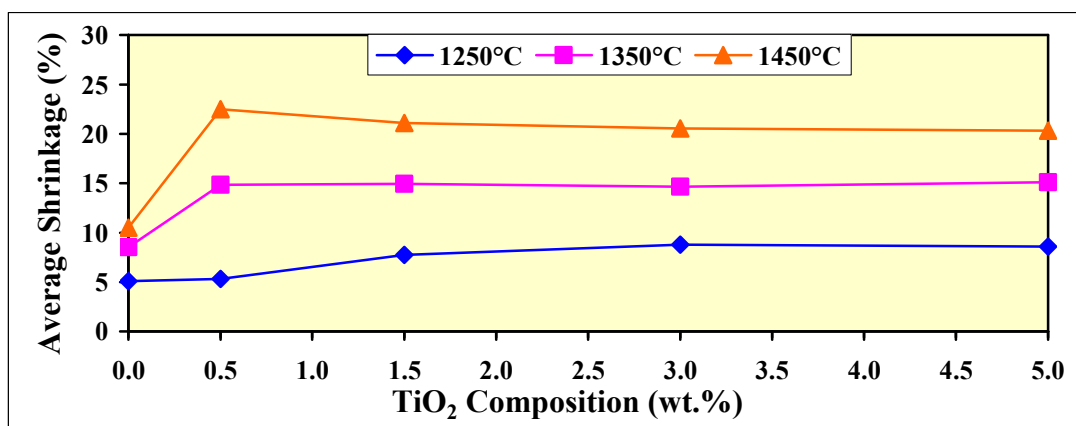
Figure 5.4: Average Shrinkage Variation of Al₂O₃ As A Function of TiO₂ Composition At Different Sintering Temperature

A comparison chart is presented in Figure 5.5 to show the advantage of using TiO_2 as the dopant to enhance the density of Al_2O_3. In general, it could be observed that TiO_2 is a beneficial additive in improving the densification of alumina ceramics at lower sintering among other counterparts. For instance, the addition of 5.0 wt.% MnO_2 on Al_2O_3 attained 3.749 g/cm^3 or 94.20% of relative density at 1350°C; however, Al_2O_3 doped with TiO_2 only requires 1250°C to achieve similar density, which is reduced for 100°C. This result has proved the efficiency of TiO_2 in lowering the required sintering temperature while maintaining the density at the same instant, which fulfills the objective mentioned in the beginning of the studies. Meanwhile, it was shown that the doping of TiO_2 and MnO_2, individually, could enhance the density gradually if compared to the densification rate of the undoped sample which is insignificant when the temperature was raised. On the contrary, the addition of MgO did not provide any positive effect to the bulk density of alumina but in turn brought down the density to be lower than that achieved by the pure alumina when the sintering temperature was increased.
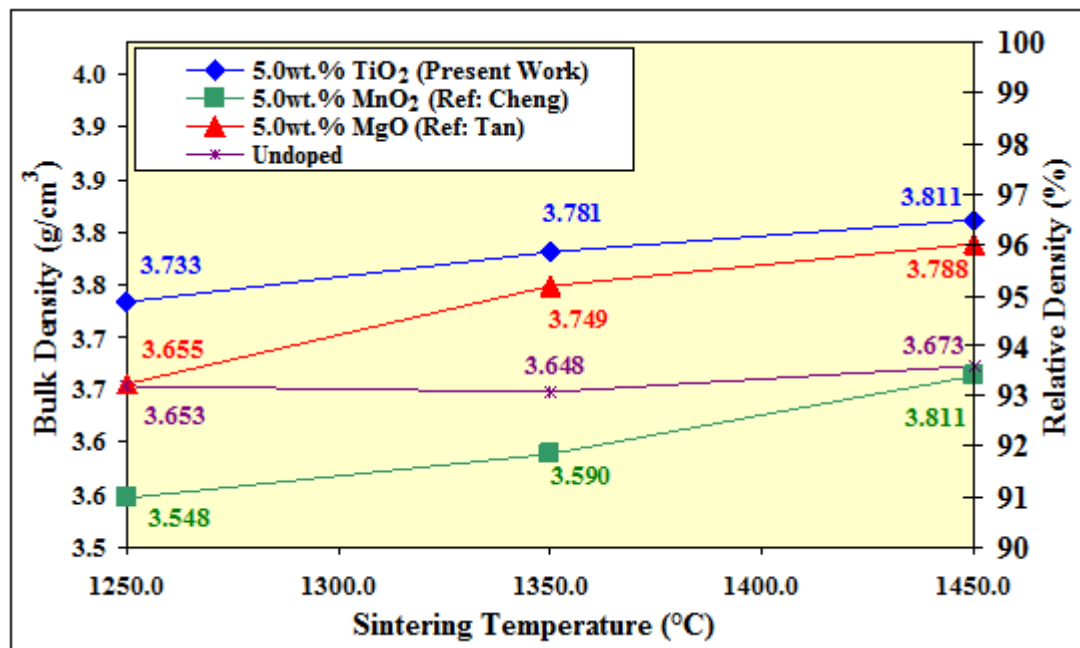
Figure 5.5: Effects of TiO_2, MnO_2 and MgO (All 5.0wt.%) On The Bulk And Relative Density of Al_2O_3 At Different Sintering Temperature

5.2　　Grain Size

From the research of Horn et al. (1995), it is noted that the increase in sintering temperature is the main contributor to the grain growth kinetics of pure alumina as well as those of TiO_2 doped alumina. Indeed, similar trend was also found in the present result as shown in Figure 5.6 in which there is a positive relationship between the sintering temperature and average grain size. For instance, the average grain size of 1.5 wt.% TiO_2 doped sample at 1450°C was found to be 0.98 μm, which is much greater than the 0.17 μm at 1250°C. Therefore, the result shows that lower sintering temperature is preferable in maintain the grain size of alumina without further grain growth. However, this benefit has to be compromised with a lower relative density of samples produced at low temperature.

Meanwhile, from the Figure 5.6, it is apparent that the doping of TiO_2 potentially increases the grain size of alumina ceramics if compared to the inconsequential increase of grain size of the undoped sample with respect to the elevation of sintering temperature. Therefore, the relationship between TiO_2 content and average grain size of alumina ceramics is presented in Figure 5.7 for further illustration. From that, the largest average grain size of 1.03 μm was found in the 1.5 wt.% TiO_2 doped alumina when it is sintered at 1450°C. Pertaining to the largest average grain size, it is noted that the largest grain of 2.48 μm was also detected in 1.5 wt.% TiO_2 doped alumina and the respective largest grain for each composition at different sintering temperatures are exhibited in Appendix A. Besides, it was shown that further increment of TiO_2 content up to 1.5 wt.% would increase the average grain size while this increment ceases when the dopant composition was added until 3.0 wt.%. Nevertheless, the grain size was enlarged again when the dopant content was added to 5.0 wt.%. This trend was noticeable at every sintering temperature.
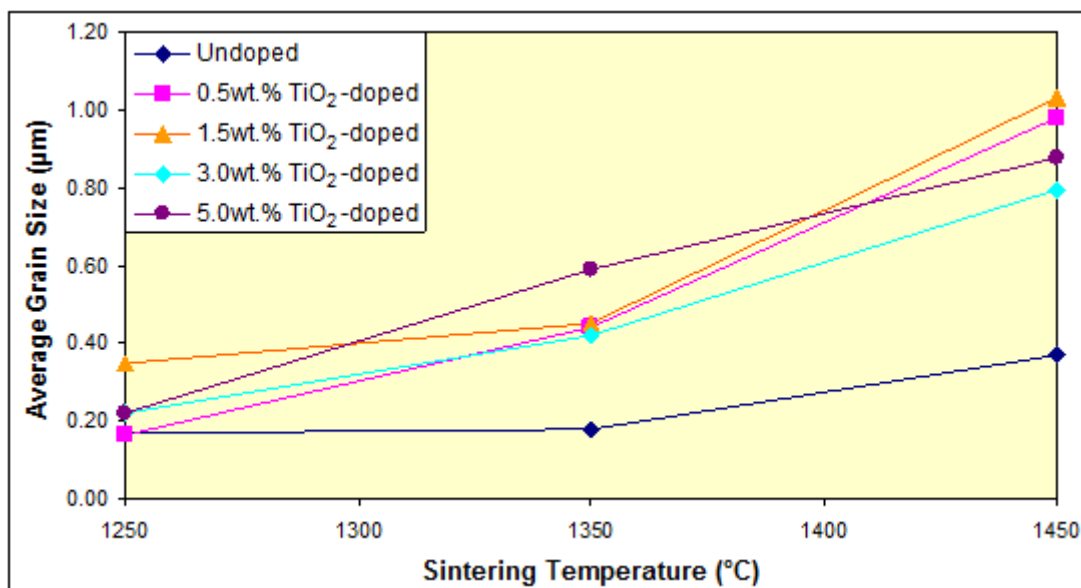
Figure 5.6: Effect of Sintering Temperature On The Average Grain Size of Al₂O₃ Doped With Different Composition of TiO₂
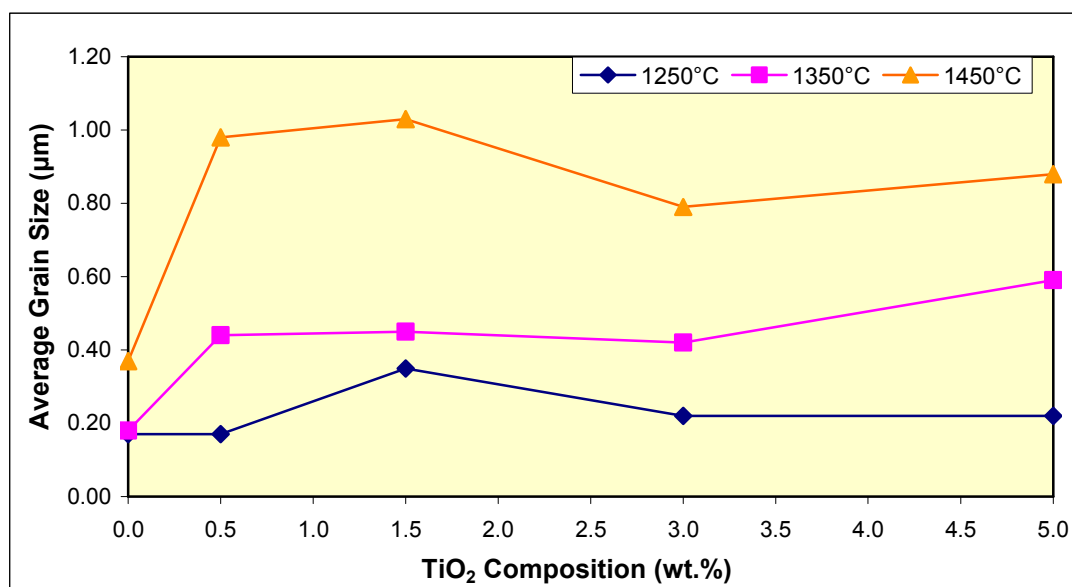
Figure 5.7: Effect of TiO₂ Composition On The Average Grain Size of Al₂O₃ At 1250°C, 1350°C and 1450°C

Furthermore, the effect of sintering temperature on the average grain size of different samples can be verified from the Scanning Electron Microscope (SEM) micrographs as depicted from Figure 5.10 to Figure 5.14. From these micrographs,

one identified commonality is the tendency of grain growth of every samples when the sintering temperature was raised from 1250°C to 1450°C. Moreover, it was found that the intragranular pores could be observed more ostensibly for higher addition levels of dopants such as 5.0 wt.% TiO_2 at 1450°C as indicated by the arrows in Figure 5.8 whereas at the same temperature, the intergranular pores in 0.5 wt.%, 1.5 wt.% and 3.0 wt.% TiO_2 doped alumina found to be reduced significantly if compared to those sintered at lower temperature, as shown in Figure 5.9. Thus, the reduction of these internal defects may lead to an enhanced densification which was found in the samples with higher addition levels and contribute to a better uniformity of the grain size distribution, which is consistent with the objective of this experiment.
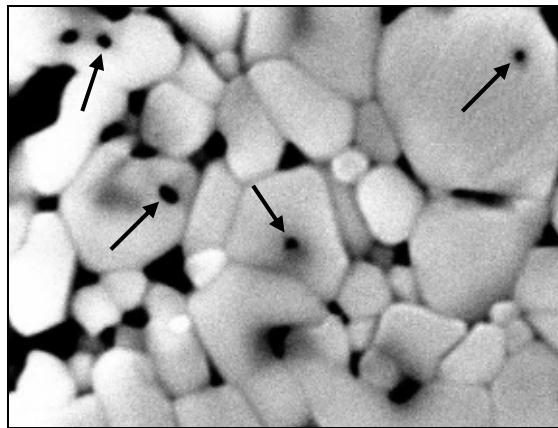
Figure 5.8: Intragranular Pores In Enlarged SEM Micrographs of 5.0 wt.% TiO_2 Doped Alumina
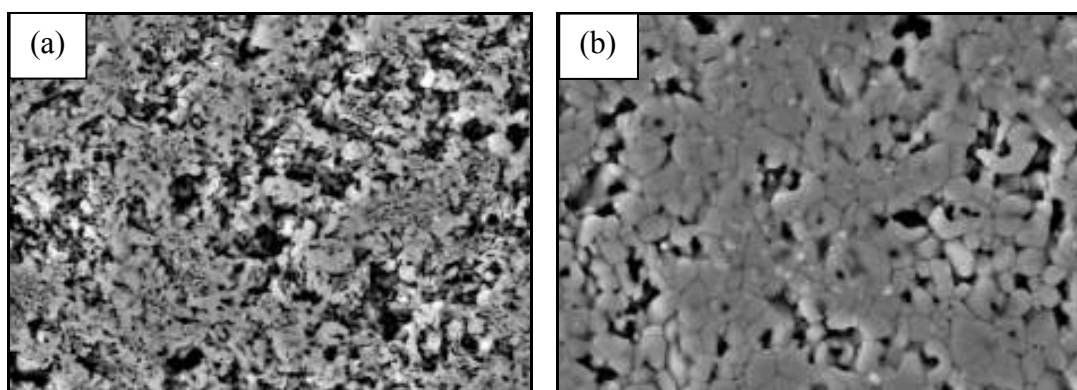
Figure 5.9: Reduction of Intergranular Pores for 1.5 wt.% TiO_2 Doped Alumina When Sintering Temperature Is Increased From (a) 1350°C to (b) 1450°C
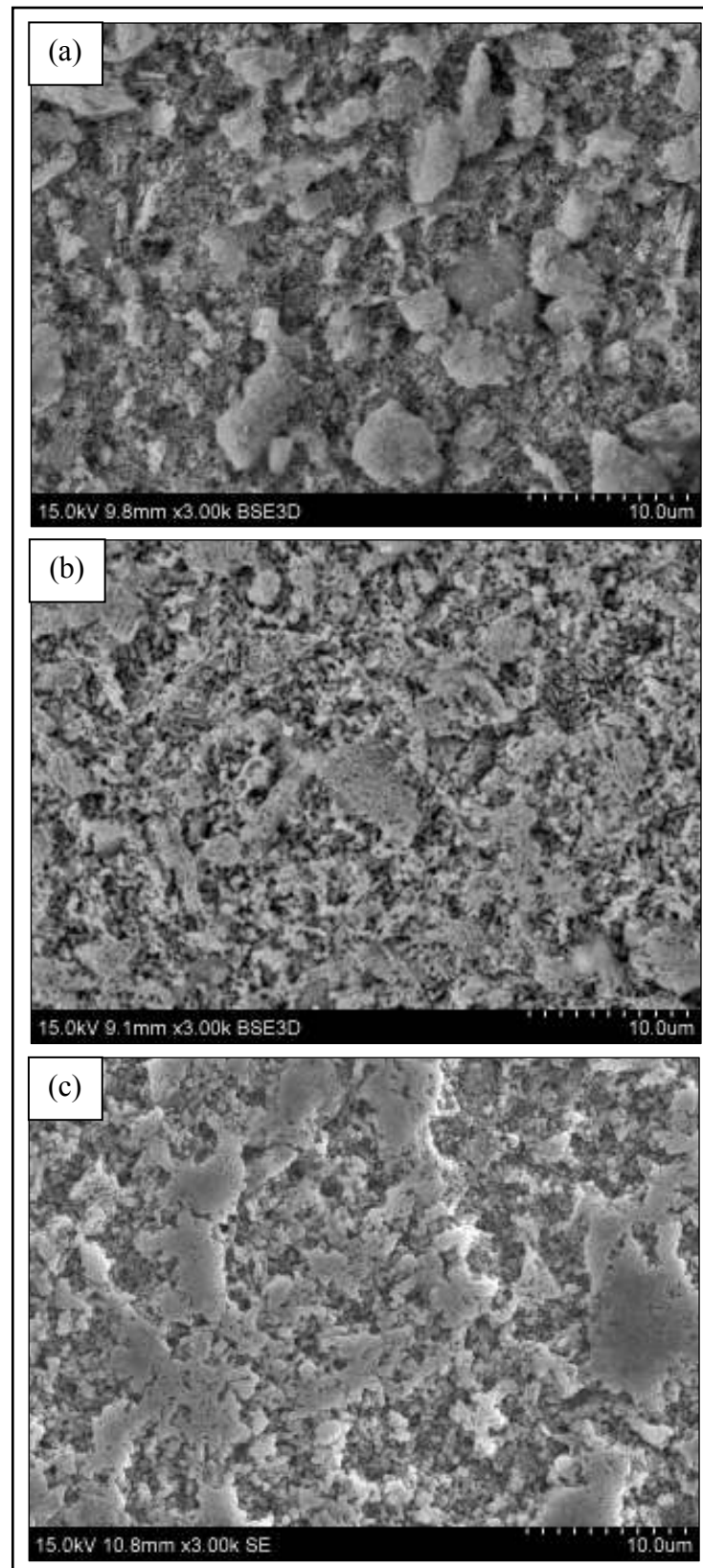
Figure 5.10: SEM Micrographs of Pure Alumina Sintered At (a) 1250°C (b)1350°C (c) 1450°C With 1 hr of Holding Time.
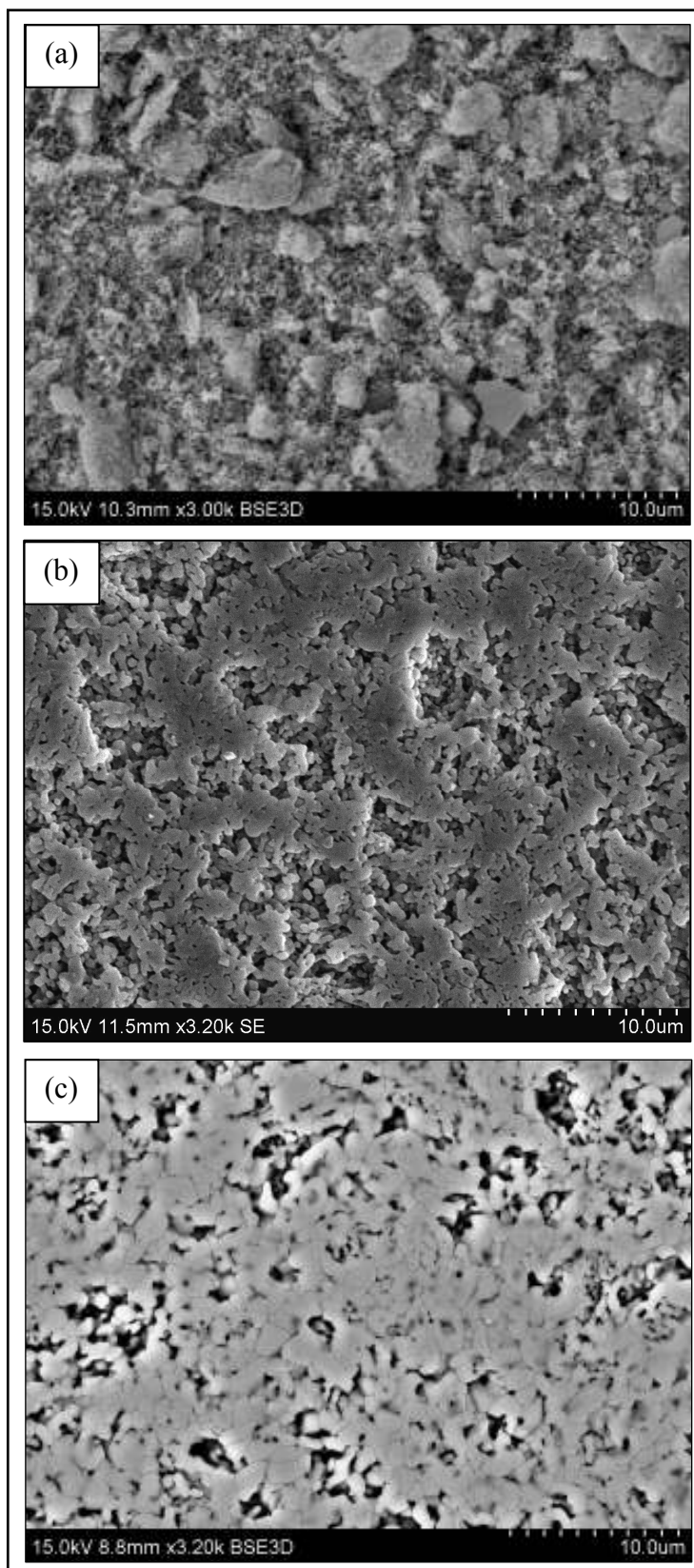
Figure 5.11: SEM Micrographs of 0.5 wt% TiO$_2$-Doped Alumina Sintered At
(a) 1250°C (b) 1350°C (c) 1450°C With 1 hr of Holding Time.
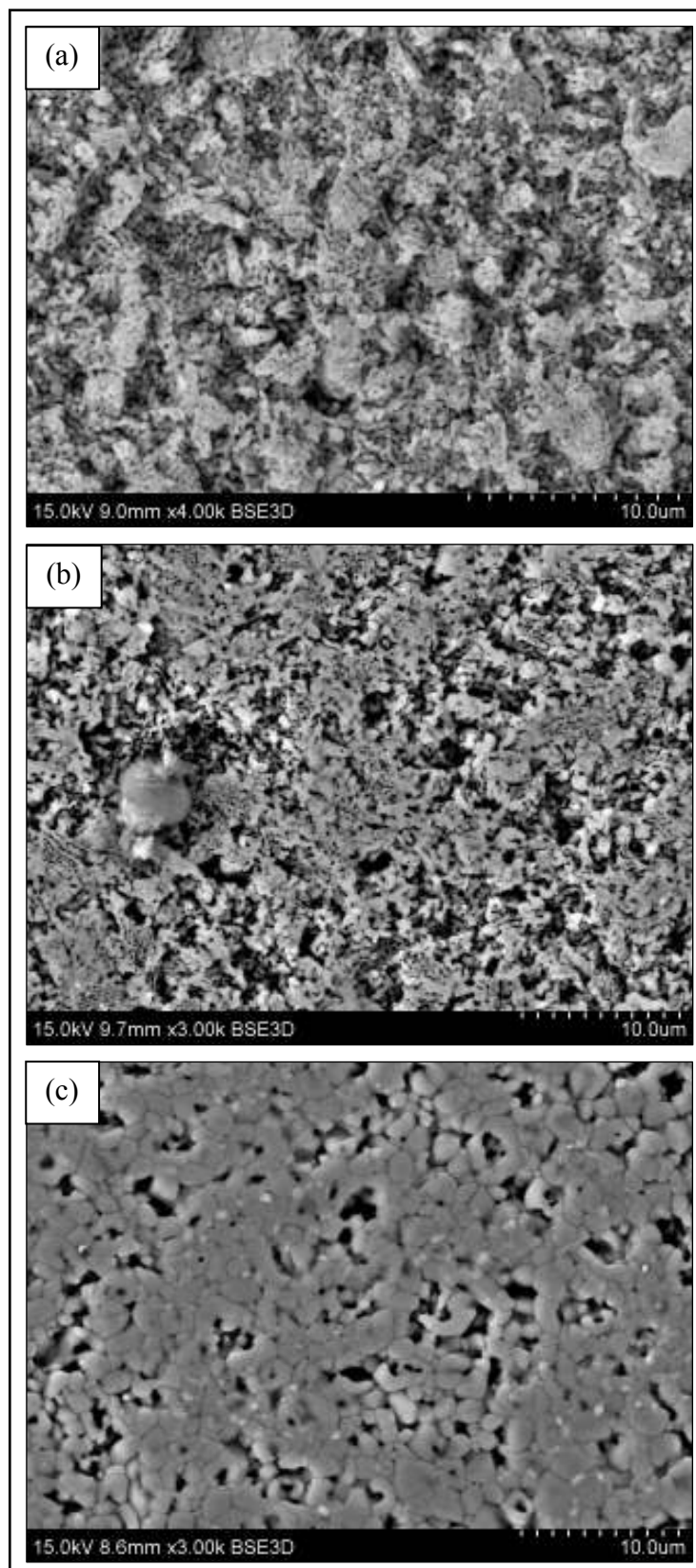
Figure 5.12: SEM Micrographs of 1.5 wt% TiO$_2$-Doped Alumina Sintered At (a) 1250°C (b) 1350°C (c) 1450°C With 1 hr of Holding Time.
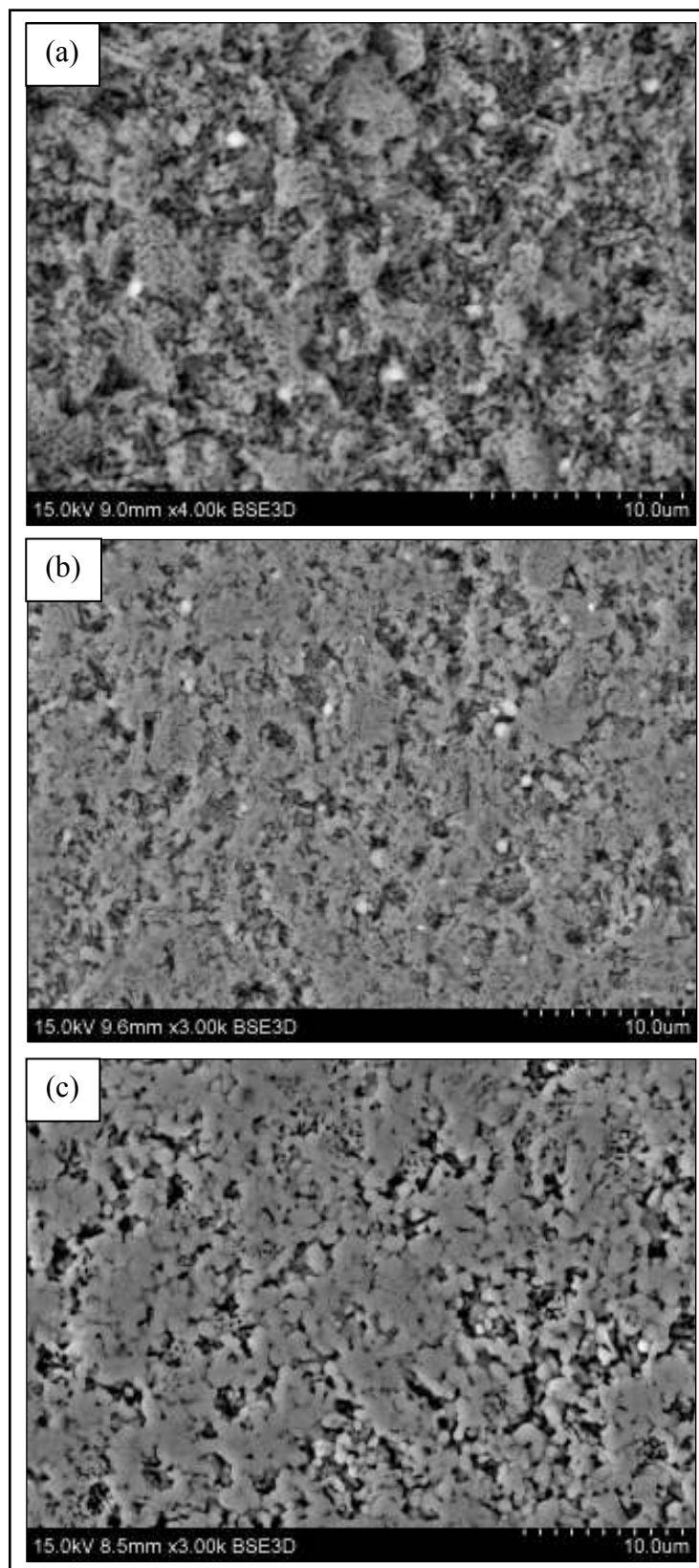
Figure 5.13: SEM Micrographs of 3.0 wt% TiO$_2$-Doped Alumina Sintered At (a) 1250°C (b) 1350°C (c) 1450°C With 1 hr of Holding Time.
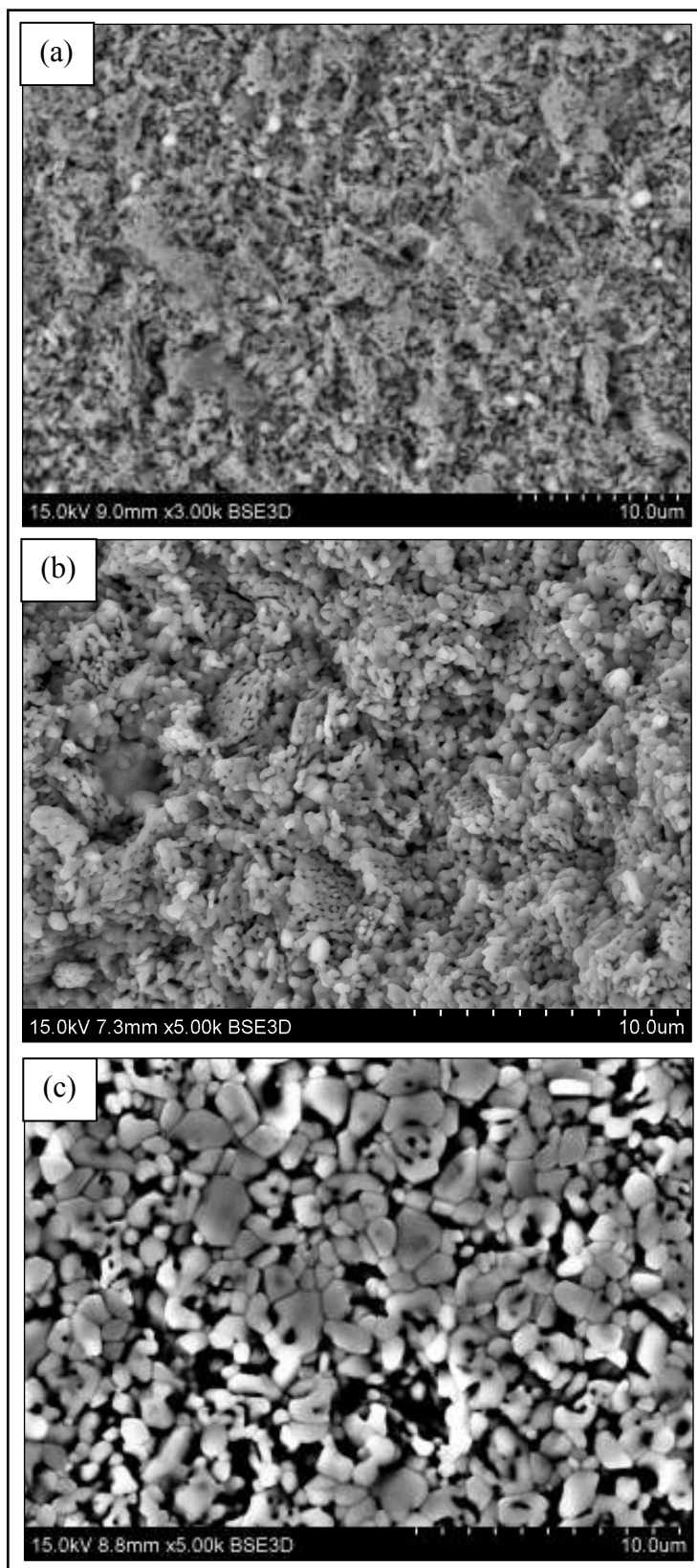
Figure 5.14: SEM Micrographs of 5.0 wt% TiO$_2$-Doped Alumina Sintered At (a) 1250°C (b) 1350°C (c) 1450°C With 1 hr of Holding Time.

By comparison, 0.5 wt.% TiO_2-doped alumina ceramics is advantageous in controlling the grain growth if compared to the sample doped with 0.5 wt.% of TiO_2 and 3.0 wt.% MnO_2. For instance, a large grain size of 2.81 μm was found to be achieved by the 0.5 wt.% TiO_2-3.0 wt.% MnO_2-doped alumina ceramics at 1450°C while at the same temperature, the grain size of 0.5wt.% TiO_2 was restricted at 0.98 μm, which is considerably lower than that attained by the mixed sample. Dissimilar to the mixed sample, alumina ceramics doped with 3.0 wt.% of MnO_2 alone confined its grain size to about 1 μm at 1450°C. From that, it is apparent that alumina ceramics of single dopant possesses a better grain growth control if compared to than that doped with two kinds of additives. The underlying reason for this scenario could be attributed to the characteristics of both TiO_2 and MnO_2 which tend to promote the grain growth under elevated sintering temperature. Thus, when these two additives were added into a base material like Al_2O_3, the multiplying effect may make the overall grain growth to be more ostensible when the sintering temperature was increased.
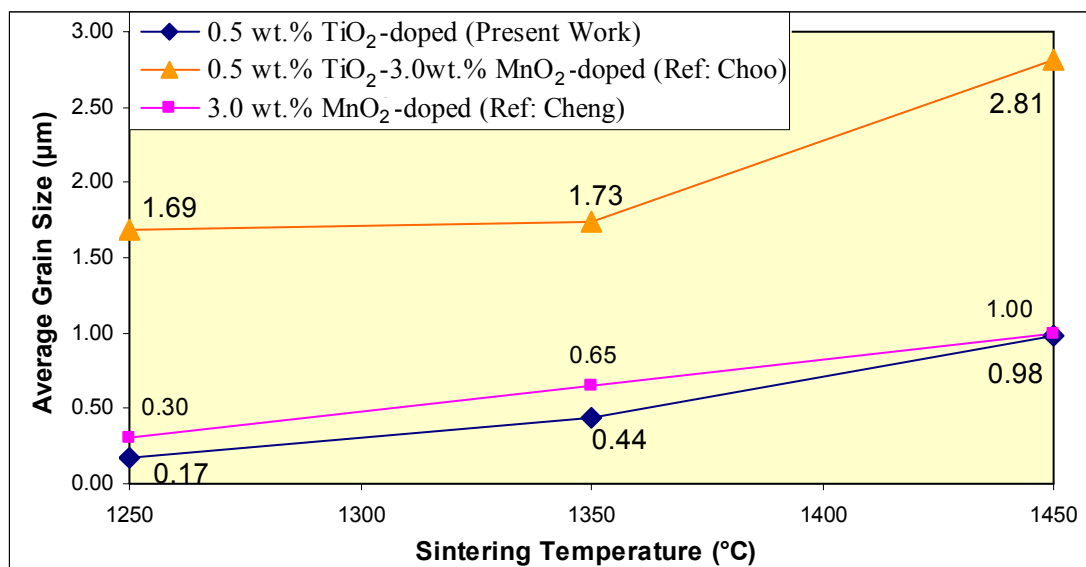
Figure 5.15: The Effect of Different Dopants On The Average Grain Size of Alumina At Different Sintering Temperature

5.3   Vickers Hardness

The effect of sintering temperature on the hardness of Al_2O_3 is presented in Figure 5.17. From that, the hardness of doped alumina samples was found to be higher than that of the undoped sample. Overall, the hardness of all samples is proportional with the sintering temperature, which is similar to the trend found in the research of Ting et al. This result can be demonstrated at 1450°C of sintering temperature in which the measured hardness was 6.64 GPa for 5.0 wt.% TiO_2 doped sample as compared to 1.79 GPa which was attained by the pure alumina. Besides, it is apparent higher sintering temperature, which is up to 1450°C in this case, is favourable to increase the hardness of all samples in comparison to those samples sintered at lowered temperature. The highest hardness of 7.6 GPa was achieved by the 0.5 wt% TiO_2 doped alumina ceramics when it was sintered at 1450°C. Nonetheless, the hardness of the 0.5wt.% TiO_2 doped sample falls slightly from 2.00 GPa at 1250°C to 1.81 GPa at 1350°C. Conversely, an insignificant increase in the hardness of undoped alumina ceramics can be observed when the sintering temperature was raised.
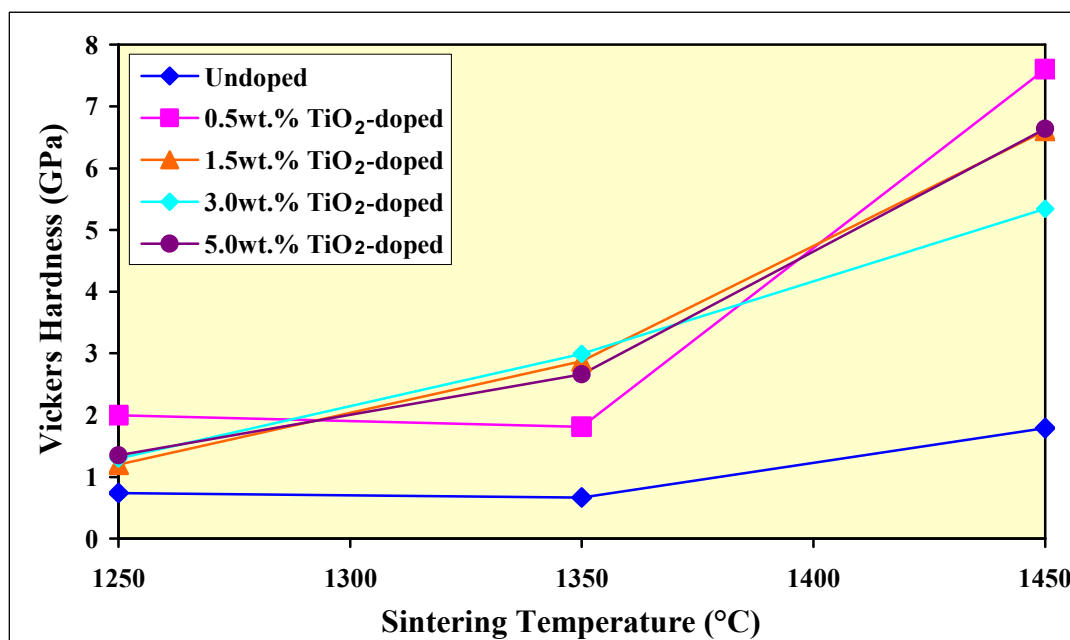
Figure 5.16: The Effect of Sintering Temperature On The Vickers Hardness of Al$_2$O$_3$ Doped With Various Composition of TiO$_2$

On the other hand, Figure 5.18 shows that further addition of TiO_2 composition beyond 0.5 wt.% on alumina ceramics would decline the hardness at both 1250 and 1450°C, whereas for 1350°C sintering, higher addition levels of dopants did not enhance the hardness but in turn dropped slightly from 2.99 GPa to 2.66 GPa when it was at 5.0 wt.% TiO_2. It seems that a reasonable explanation for the reduction of hardness at 1450°C may be related to the appearance of secondary phase, Aluminium Titanate, Al_2TiO_5, on 1.5 wt.% TiO_2 doped alumina as observed by the XRD analysis (see Figure 5.26(f)). This assumption was further verified when more secondary phase are detected in the 3.0wt.% TiO_2 sample which further reduce its hardness from 6.61 GPa at 1.5wt.% to 5.34 GPa. This result is in a good agreement with the variation reported by Wang et al. which stated that the existence of secondary phase evolution such as Al_2TiO_5 with low elastic modulus may decrease the hardness of alumina ceramics. Subsequent to this decrement, the hardness was, nevertheless, increased again to 6.64 GPa when the sample was added with 5 wt.% TiO_2. Noticeably, the hardness of the samples, which were sintered at 1350°C, did not assist in enhancing the hardness but remained idle when the TiO_2 composition is increased up to 1.5 wt% and above.
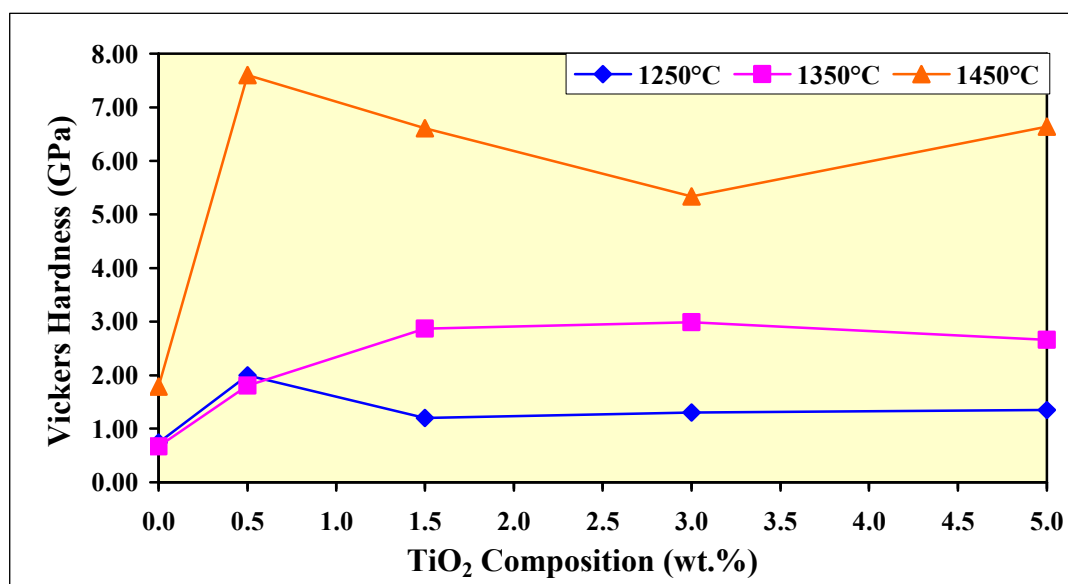
Figure 5.17: Effect of TiO_2 Composition On The Vickers Hardness of Al_2O_3 At Different Sintering Temperature

The hardness of alumina ceramics doped with different amount of TiO_2 and MgO, respectively, was exhibited in Figure 5.19. From that, it could be noticed that TiO_2 outshines MgO to serve as a good dopant in promoting the hardness of alumina ceramics. For instance, the highest hardness that could be attained by the TiO_2 doped sample is 7.6 GPa, which is much greater than that of the MgO doped alumina which only achieved 2.44 GPa. As mentioned in previous section, the weakening of hardness at 1.5 wt.% of TiO_2 may associated with the existence of secondary phase, Al_2TiO_5, at 1450°C which tends to reduce the hardness of base material (Wang et al., 2008). However, the decrement in hardness of TiO_2-doped sample remained higher than those of the samples doped with MgO additive which only exhibits an insignificant variation of Vickers hardness. Moreover, it was observable that the addition of MgO up to 5.0 wt.% in Al_2O_3 was detrimental to the hardness of alumina ceramics as the achieved hardness at this composition, 1.68 GPa, was even lower than that of the pure alumina, which attained 1.79 GPa, under same condition. On the contrary, the addition of TiO_2 at different composition could generally enhance the hardness of alumina which was higher than those of the undoped samples.
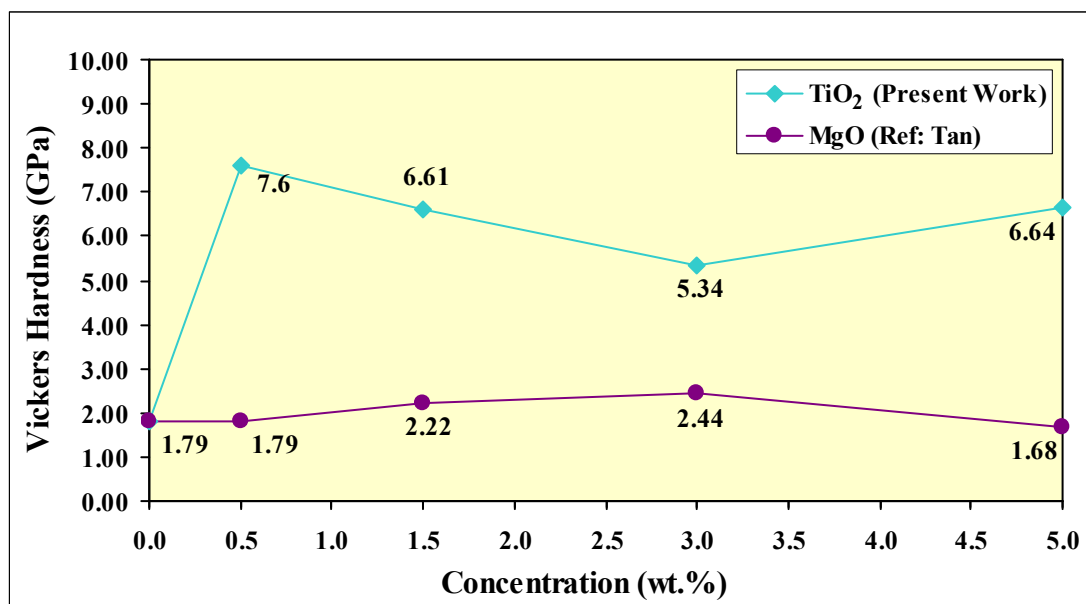
Figure 5.18: Effects of TiO₂ and MgO Addition At Different Concentration On The Vickers Hardness of Alumina Ceramics At 1450°C.

5.4 Young's Modulus

A general observation that can be made from Figure 5.20 is that the addition of TiO_2 dopant would increase the modulus of elasticity of Al_2O_3 regardless of sintering temperature employed. This result can be validated through the research of Ting et al. which claimed that the TiO_2 has a positive effect on the Young's modulus of alumina ceramics (Ting et al., 2008). From that, it was found that Al_2O_3 doped with 0.5 wt.% TiO_2 could achieve the highest Young's Modulus, which is 267.74 GPa at 1450°C. Other than 0.5 wt.% TiO_2, the samples with higher dopant concentration could also attain Young's modulus in the range between 170 GPa and 220 GPa at the same sintering temperature, which is higher than the undoped sample that only attained approximately 50 GPa at 1450°C.
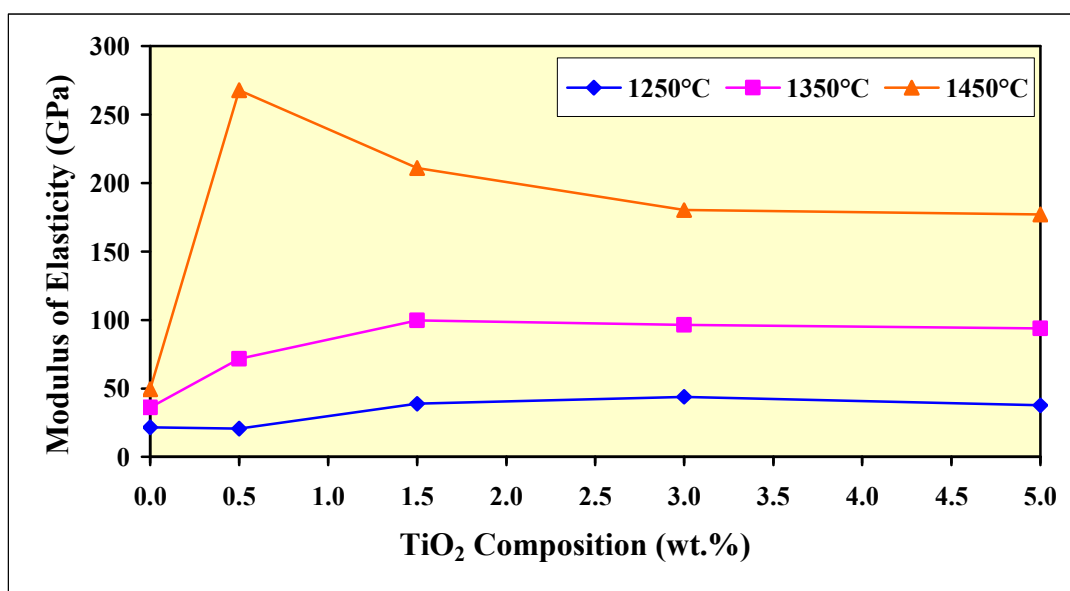
Figure 5.19: Effect of TiO2 Composition On The Young's Modulus of Al2O3 At Different Sintering Temperature

Noteworthily, the variation of Young's modulus as a function of TiO_2 composition at 1450°C is similar to the trend of the hardness at the same temperature whereby both of them experienced a drop at 1.5 wt.% TiO_2. Thus, it was believed that presence of secondary phase, Al_2TiO_5, would affect the Young's modulus as well when the samples were sintered at high temperature such as 1450°C. Another

visible trend that can be observed is that the Young's modulus of the samples were seemed to be constant when the TiO_2 concentration was increased up to 1.5 wt.% at both 1250°C and 1350°C. Nevertheless, the Young's Modulus of the samples at 1450°C declined significanly when the TiO_2 concentration was increased up to 1.5 wt.% and finally reached a stagnation at 3.0 wt.% and above.

Likewise, the effect of sintering temperature on the variation of Young's modulus of all composition studied is analogous with the bulk density trend. In other words, the rise in sintering temperature would enhance the Young's Modulus of Al_2O_3. By referring to Figure 5.21, it was noticed that the Young's Modulus of the samples, which were sintered at 1450°C, was found to be higher in comparison to those sintered at lower temperature. From that, the beneficial effect of higher sintering temperature could be observed through the 0.5 wt.% TiO_2 doped sample in which its Young's Modulus raised remarkably from 71.75 GPa at 1350°C to the maximum value of 267.74 GPa at 1450°C. On the other hand, the samples with higher dopant composition show a slower increasing rate of Young's modulus at the same temperature interval if compared to that of the 0.5 wt.% TiO_2 doped sample whilst the ascending rate of Young's Modulus of the undoped sample was insignificant when the sintering temperature was increased.
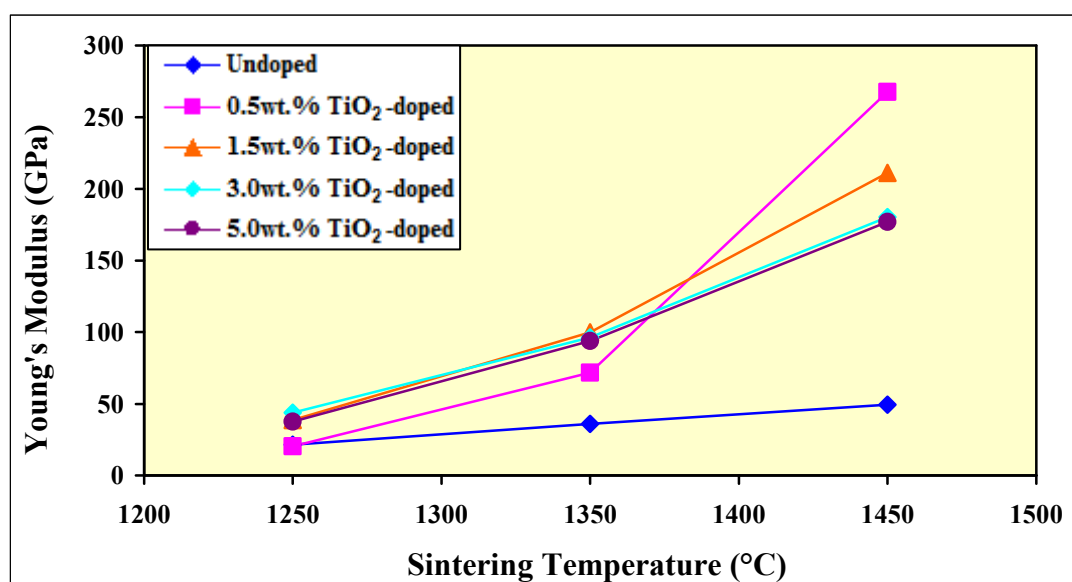
Figure 5.20: Effect of Sintering Temperature On The Young's Modulus of Al₂O₃ Doped With Various Composition of TiO₂

As shown in Figure 5.22, a comparison was made between TiO_2, MnO_2 and MgO to identify their respective effects on the hardness of alumina ceramics at 1450°C sintering. In general, it could be seen that the addition of TiO_2 is proficient in promoting Young's modulus of alumina. For instance, the highest modulus of elasticity of TiO_2 reached 267.74 GPa at 0.5 wt.%, which is greater if compared to that of the MnO_2 and MgO, which achieved 244.13 GPa and 63.63 GPa at their respective 3.0 wt.% contents. Therefore, if the main concern is emphasized on a high Young's modulus, 0.5 wt.% TiO_2 is more suitable than its higher concentration due to the reduction of Young's modulus for TiO_2 at higher addition level as shown in Figure 5.22. Meanwhile, an insignificant increase of Young's modulus was found in the case of MgO dopant while the addition of MnO_2 could gradually increase the modulus of elasticity but none of the results could exceed the maximum value which was achieved by 0.5 wt.% TiO_2 doped alumina. From that, the beneficial effect of TiO_2 especially for the 0.5 wt.% addition in enhancing the Young's modulus of alumina ceramics has been revealed.
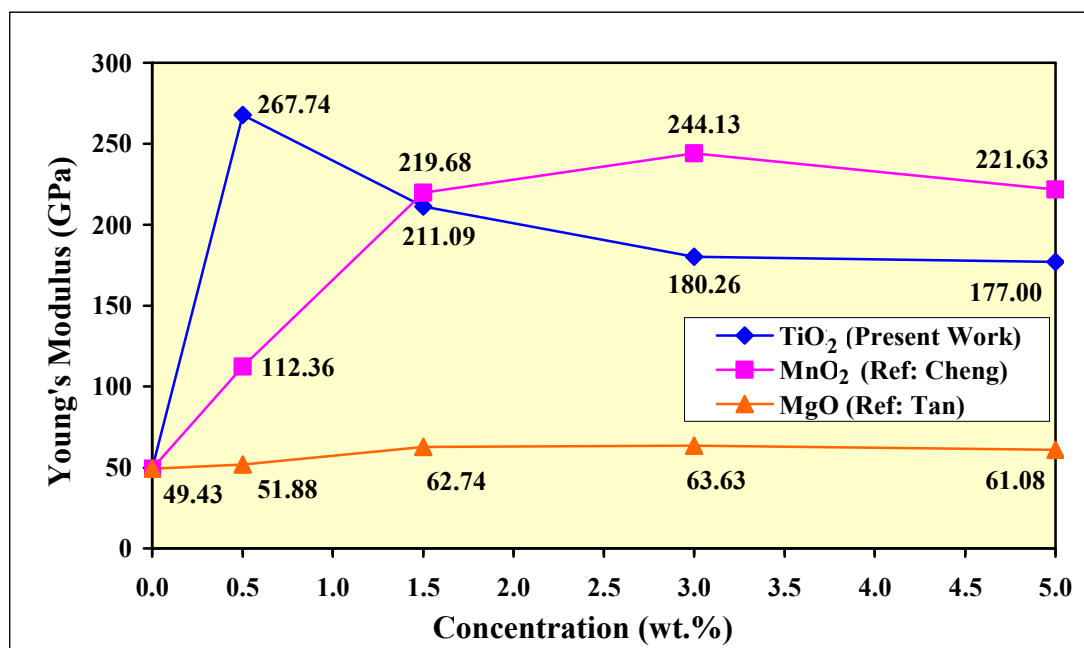
Figure 5.21: Effects of TiO_2, MnO_2 and MgO Addition At Different Composition On Young's Modulus of Alumina Ceramics At 1450°C.

5.5   X-Ray Diffraction (XRD) Analysis

There were three elements found in the samples, which are the major compound, Aluminium Oxide (Al_2O_3), the undissolved dopant, Rutile (TiO_2), and the secondary phase, Aluminium Titanate (Al_2TiO_5). As illustrated in Figure 5.23, TiO_2, in the form of anatase, is dissolved completely in alumina ceramics to form a solid solution before sintering since no new peaks are discovered while the peaks of all samples are almost identical to the standard peak of the dominant compound, Al_2O_3. After sintering, it is apparent that none of insoluble rutile and secondary phases were found at any sintering temperature for undoped and 0.5 wt.% TiO_2-added sample.

From Table 5.1, it can be observed that the solubility limit of TiO_2 occurs when the concentration was added up to 1.5 wt.%, therefore leads to the appearance of insoluble rutile in higher addition levels such as 3.0 wt.% and 5.0 wt.% of TiO_2 at every sintering temperature. This indicates that the TiO_2 that appeared in the anatase form before sintering had been transformed into rutile form at 1250°C and at higher sintering temperatures. By matching the sample's intensity with the standards from International Centre for Diffraction Data (ICDD), the presence of secondary phase can be detected at 1450°C for higher addition levels of TiO_2. For instance, the intensity of the peak of the secondary phase can be identified at approximately 34 and 48 degrees of the 3.0 wt.% and 5.0 wt.% of TiO_2 addition as shown in XRD analysis in Figure 5.26. Besides, insignificant amount of secondary phase can also be found at 1.5 wt.% of TiO_2 concentration.

Table 5.1: Summary of Elements Present In Samples Added With Different Amounts of TiO$_2$ at 1250°C, 1350°C and 1450°C
(A = Aluminium Oxide, Al$_2$O$_3$, R = Titanium Oxide, TiO$_2$ (Rutile), T = Aluminium Titanate, Al$_2$TiO$_5$)

Sintering Temperature (°C)	TiO$_2$ Composition (wt.%)				
	0.0	0.5	1.5	3.0	5.0
Before Sintering	A	A	A	A	A
1250	A	A	A+R	A+R	A+R
1350	A	A	A+R	A+R	A+R
1450	A	A	A+T	A+R+T	A+R+T
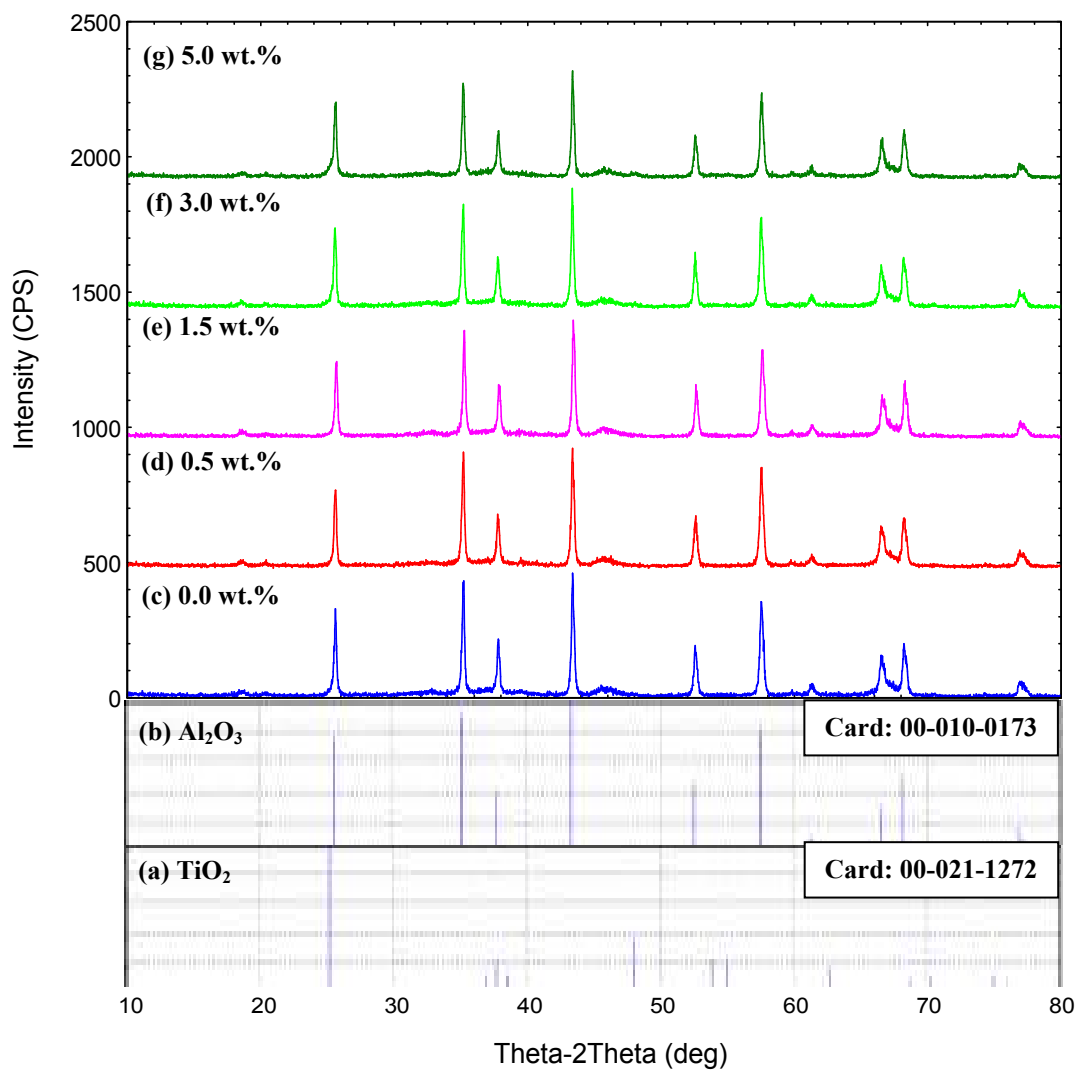
Figure 5.22: XRD patterns of (a) TiO₂ (Anatase) (b) Al₂O₃ (c) non-added, (d) 0.5 wt.%, (e) 1.5 wt.%, (f) 3.0 wt.%, (g) 5.0 wt.% TiO₂ doped powder
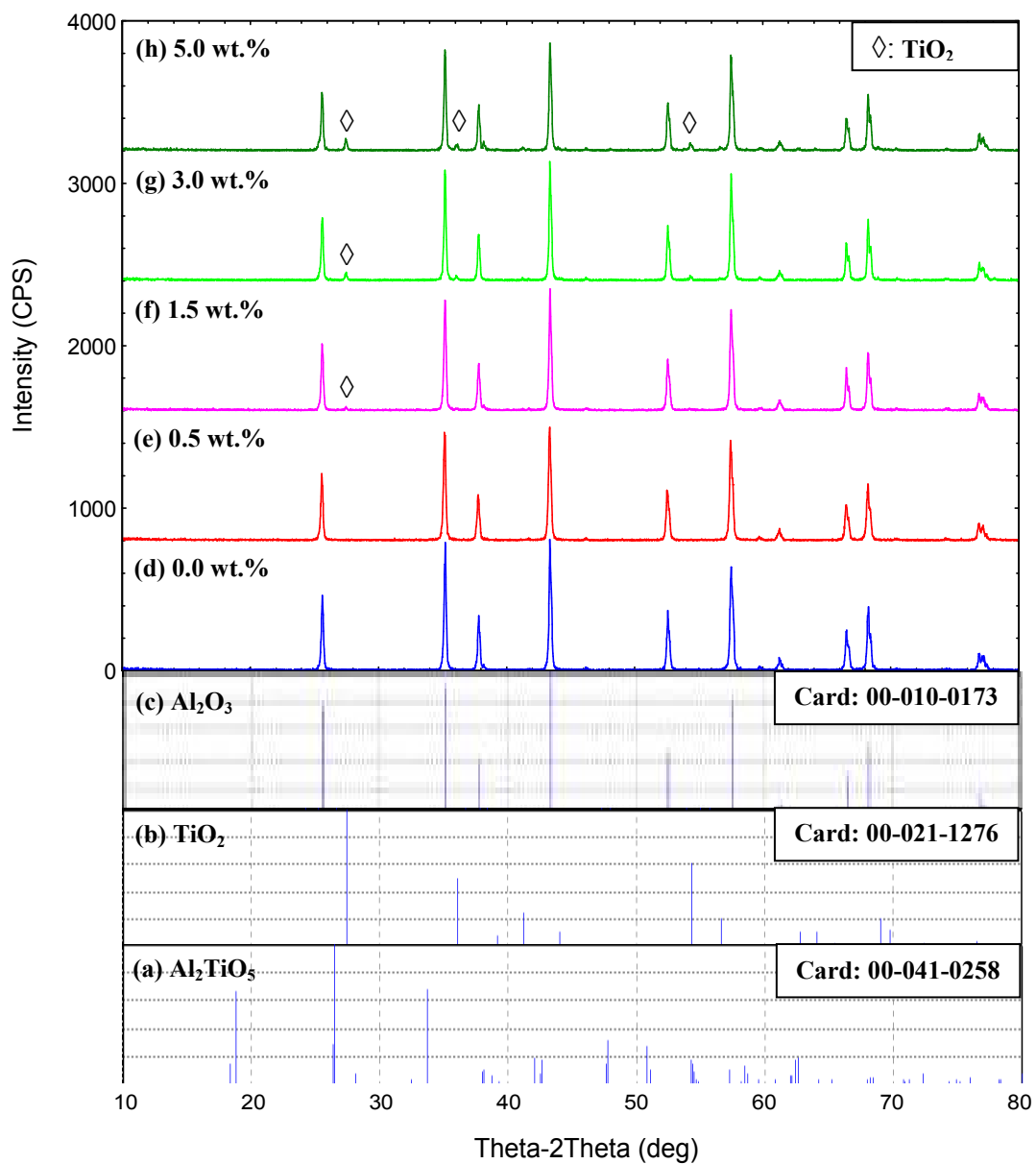
Figure 5.23: XRD patterns of (a) Al₂TiO₅ (b) TiO₂ (Rutile) (c) Al₂O₃ powder (d) non-added, (e) 0.5 wt.%, (f) 1.5 wt.%, (g) 3.0 wt.%, (h) 5.0 wt.% TiO₂ doped powder sintered at 1250°C
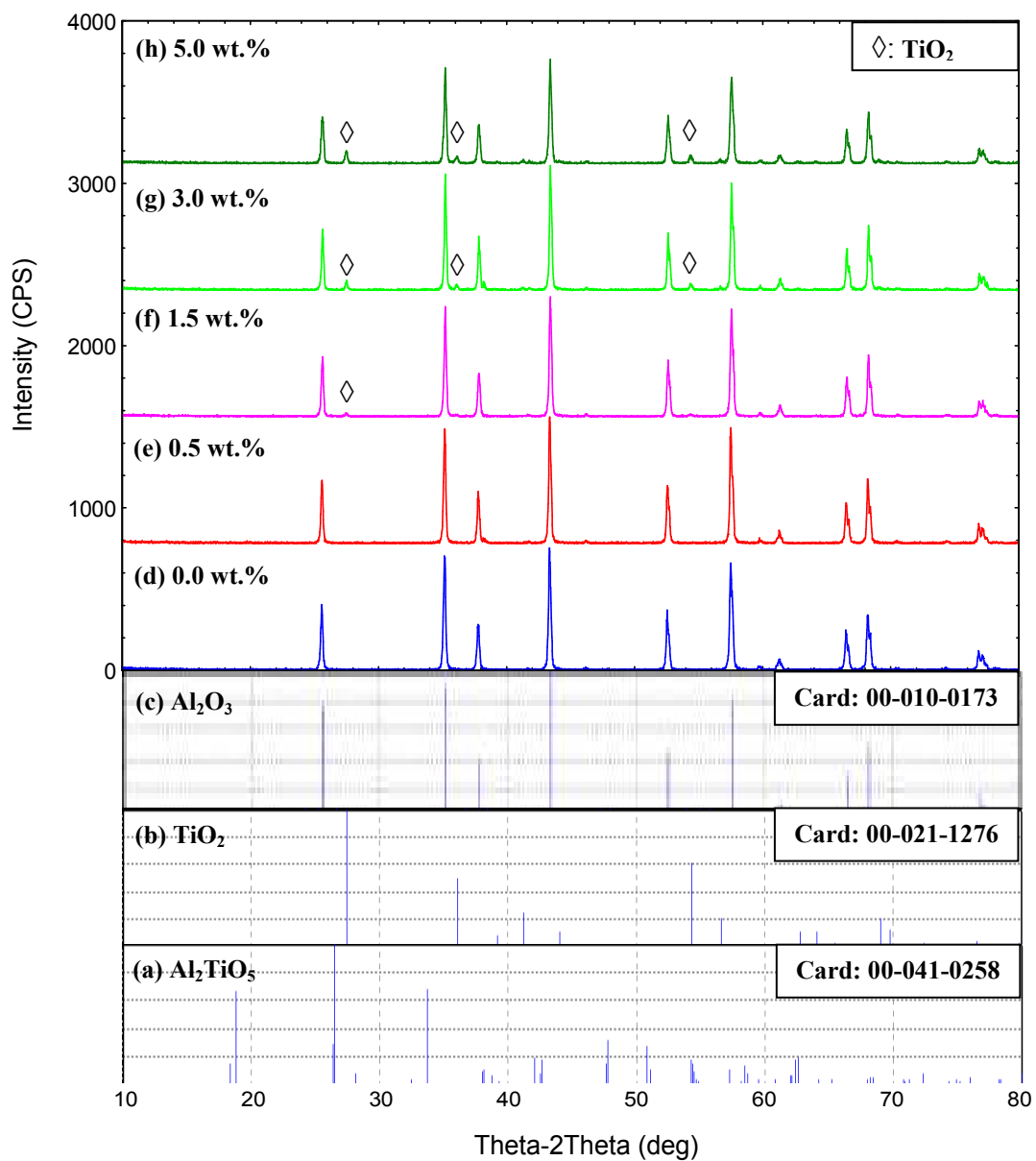
Figure 5.24: XRD patterns of (a) Al₂TiO₅ (b) TiO₂ (Rutile) (c) Al₂O₃ powder (d) non-added, (e) 0.5 wt.%, (f) 1.5 wt.%, (g) 3.0 wt.%, (h) 5.0 wt.% TiO₂ doped powder sintered at 1350°C
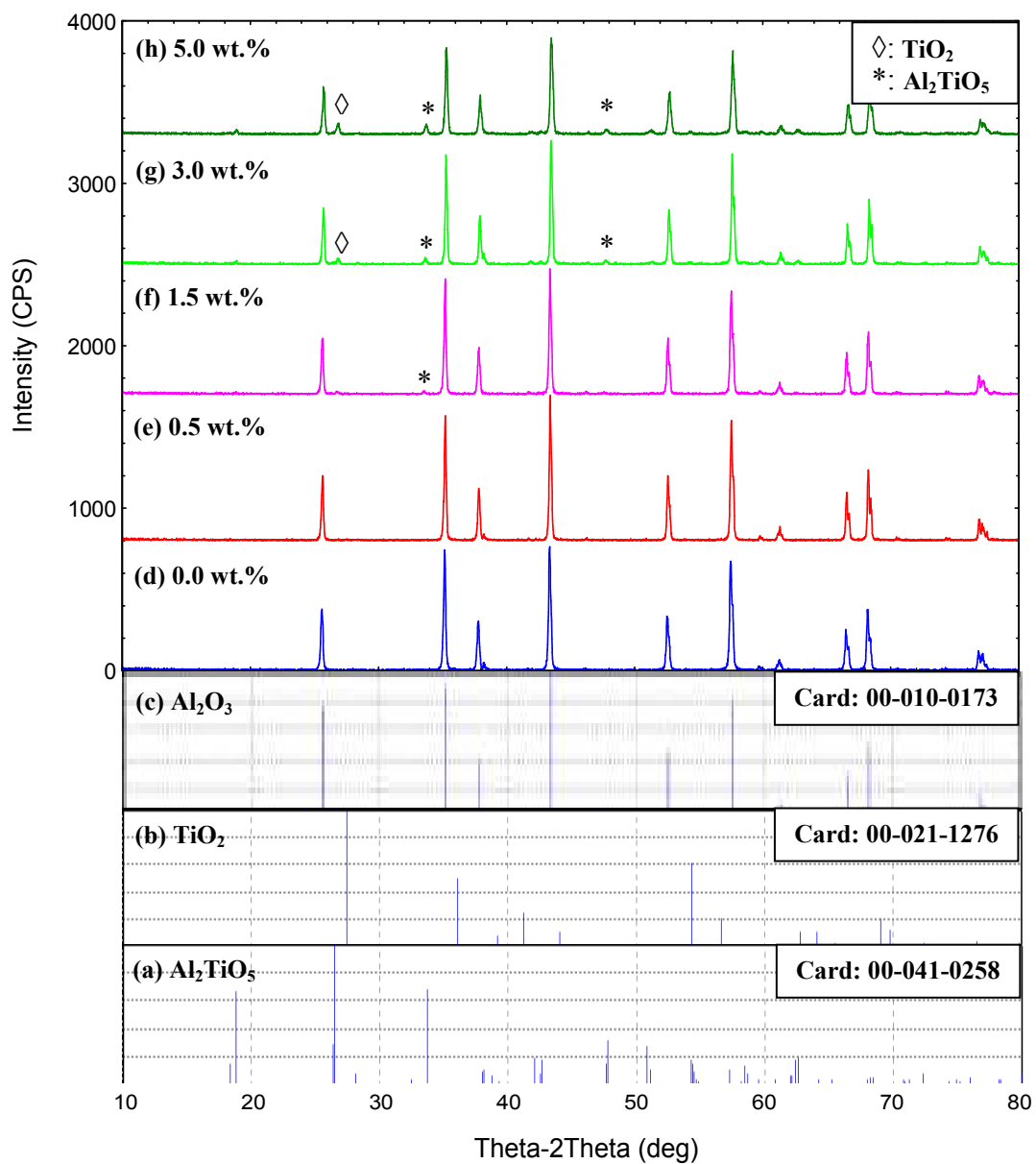
Figure 5.25: XRD patterns of (a) Al₂TiO₅ (b) TiO₂ (Rutile) (c) Al₂O₃ powder (d) non-added, (e) 0.5 wt.%, (f) 1.5 wt.%, (g) 3.0 wt.%, (h) 5.0 wt.% TiO₂ doped powder sintered at 1450°C

CHAPTER 6

CONCLUSION AND RECOMMENDATION

6.1   Conclusion

Small addition of Titanium Oxide, TiO_2 up to 5.0 wt.% have been found to be beneficial in lowering the sintering temperature, as from 1450°C to 1350°C to achieve a relatively high densification, which is 95% of theoretical density. Generally, the relative density of Al_2O_3 increases with the sintering temperature and the amount of TiO_2 addition. All the TiO_2 doped Al_2O_3, which were sintered at 1450°C, could achieve approximately 96% of theoretical density if compared to 92.29% for the undoped ceramics under the condition. Meanwhile, the highest density that could be attained was occurred at 0.5 wt.% TiO_2 doped Al_2O_3 when it was sintered at 1450°C.

The grain size of Al_2O_3 shows a positive relationship with the sintering temperature while the effect of TiO_2 additive does increase the grain growth up to 1.5 wt.% of concentration. However, the grain size experiences a sudden drop at intermediate concentration of 3.0 wt.% TiO_2 addition. The largest average grain size, 1.03 μm, was found to be occurred at 1.5 wt.% TiO_2 when sintered at 1450°C while the largest grain recorded, 2.48 μm, was also discovered in the same composition and temperature. The presence of intragranular pores is noticeable for higher addition levels of dopants such as 5.0 wt.% TiO_2 at 1450°C whilst at the same temperature, the intergranular pores in 0.5 wt.%, 1.5 wt.% and 3.0 wt.% TiO_2 doped alumina was found to be reduced significantly, thus contributes to a relatively homogeneous grain size distribution.

An increase in sintering temperature would also boost the hardness and Young's Modulus of Al_2O_3. The addition of 0.5 wt.% TiO_2 was noted for its capability to achieve the highest hardness and Young Modulus of alumina ceramics, which were 7.6 GPa and 267.74 GPa , respectively when it was sintered at 1450°C. Besides, the consistent presence of Aluminium Titanate, Al_2TiO_5, as the secondary phase generated by high TiO_2 addition levels and higher sintering temperature such as 1450°C, would decrease the hardness gradually from 7.6 GPa at 0.5 wt.% TiO_2 to 5.34 GPa at 3.0 wt.% TiO_2 due to its characteristic of low elastic modulus.

Therefore, by reviewing to the results, the objective of this final year project is fulfilled because the beneficial effects of incorporating small amounts of TiO_2 in terms of economic aspect and its efficiency are evidenced in the quest of enhancing the densification of alumina at low temperature TiO_2 addition without sacrificing other properties such as grain size, hardness and Young's modulus.

6.2   Recommendation

In present work, the powder preparation method comprises ultrasonification and ball milling of the mixture prior to the drying process to produce a well-dispersed mixture. Nevertheless, these methods might not be sufficiently effective in order to produce a mixture with high homogeneity especially in the doping of minor amount of submicron particles. Therefore, colloidal method is strongly recommended because it is particularly useful in the doping of alumina with less than 1% of additive. If colloidal method is employed for the powder mixing process, the desired dopant, which is Titanium oxide in this case, could be added in the form of a salt solution such as nitrates, sulphates and acetates so that more homogeneous microstructures and properties could be obtained (Toy et al., 1995).

Microwave sintering can be used as an effective mean to overcome the inhomogeneous grain size distribution which is attributed by the uneven heat dissipation. This problem is often encountered by the samples which are sintered with conventional sintering since this sintering technique involves heat conduction

which is transmitted from exterior into interior part of the sample. Hence, the covered bottom surface of the sample that directly lies on the foam may receive less sintering heat if compared to that of the exposed surface. On the contrary, the introduction of microwave sintering solves this problem by generating uniform microwave heat dissipation from all directions and shortening the sintering period to inhibit further grain growth, thereby preserving microstructural refinement on both surfaces of the samples.

Another area which requires improvement is the technique of measuring the Vickers hardness. In present work, the hardness was computed by observing through a built-in microscope attached on the Microhardness tester that requires a lot of eye-hand coordination. However, the accuracy of the data was often being affected as some of the pyramidal diamond indentation appear indistinctly due to insufficient applied force or uneven sample's surface. Furthermore, parallax error may occur as the assessing method for each person varies between one another. Thus, the use of a computer with monitoring screen that is connected to the microhardness tester would ease the observation as well as increase in the precision of measurement by eliminating human mistakes.

REFERENCES

Aalund, R. (2009). Industrial Heating. Unveiling Spark Plasma Sintering High Throughput Processing. Retrieved, 24th August, 2010, from http://www.industrialheating.com/Articles/Feature_Article/BNP_GUID_9-5-2006_A_10000000000000709694

American Ceramic Society. (2010). History of Ceramics. Retrieved July 3, 2010, from http://ceramics.org/learn-about-ceramics/history-of-ceramics/

Auerkari, P. (1996). Mechanical and physical properties of engineering alumina ceramics. Julkaisija-Utgivare Publisher.

A to Z of Materials. (2010). Sintering: Hot Pressing. Dynamic Ceramic Precision Engineering Ceramic Solutions. Retrieved, 24th August, 2010, from http://www.azom.com/article.aspx?ArticleID=4123

Bae, S. I., & Baik, S. (1994). Critical Concentration of MgO for the Prevention of Abnormal Grain Growth in Alumina. J. Am. Ceram. Soc. 77 [10] 2499-504.

Bansal, N. P., & Singh J. P. (2009). Processing and Properties of Advanced Ceramics and Composites: Ceramic Transactions, Volume 203. John Wiley and Sons.

Barsoum, M. W. (2003). Fundamentals of ceramics. Institute of Physics Publishing.

Basu, B., Lee, J. H., & Kim, D. Y. (2004). Development of Nanocrystalline Wear-Resistant Y-TZP Ceramics. J. Am. Ceram. Soc., 87 [9] 1771–1774.

Bengisu, M. (2001). Engineering Ceramics. Microwave Sintering. Springer.

Biamino, S., Fino, P., Pavese, M., Badini, C. (2006). Alumina–zirconia–yttria nanocomposites prepared by solution combustion synthesis. Ceram. Int. 32, 509–513.

Black, J., & Hastings G. W. (1998). Handbook of biomaterial properties, 344. Springer.

Brevier Technical Ceramics. (2004). Oxide Ceramics. Technical Commission of the Technical Ceramics Section of the Association of Ceramics Industries (VKI)

Bodišová, K., Šajgalik, P., Galusek D., Švancarek, P. (2007) Two-stage sintering of alumina with submicronmeter grain size, J. Am. Ceram. Soc. 90 (1) 330-332

Callister, W. D. (2005). Fundamentals of materials science and engineering: An integrated approach. John Wiley & Sons.

Callister, J. W. D. (2007). Material Science and Engineering: An Introduction. (7th Ed.). Ceramic Materials Structures and Properties, Applications and Processing. John Wiley & Sons.

Carniglia, S. C., & Barna, G. L. (1992). Handbook of industrial refractories technology: principles, types, properties, and applications. Principle of Thermal Stability, 162. William Andrew Publishing.

Carter, C. B., & Norton, M. G. (2007). Ceramic materials: science and engineering. Chapter 2: Some History. Springer.

Chattopadhyay, R. (2004). Advanced thermally assisted surface engineering processes. Chapter 13 Hot Isostatic Press. Springer.

Chen, C. P., Yang, H. Z., Gao, J. X., Sun, H. W., Hu, X. (2009). Densification behaviour and microstructural evolution of TiO2/CAS-incorporated alumina. Ceramics International 35 (2009) 585–590. Elsevier.

Chen, I. W., Wang, X. H. (2000). Sintering dense nanocrystalline ceramics without final-stage grain growth. Nature, 404, 168–171.

DIANE Publishing Company. (1993). New Materials Society, Challenges and Opportunities: New Materials Science and Technology. DIANE Publishing.

Fan, J. H., & Chen, H. (2008). Advances in Heterogeneous Material Mechanics. Lancaster: DEStech Publications, Inc.

Goldman, A. (2005). Modern ferrite technology, Volume 2005. Springer Science & Business.

Groover, M. P.. (2010). Fundamentals of Modern Manufacturing: Materials, Processes, and Systems. John Wiley and Sons

Guo, J. K., & Tuan, J. H. (2004). Multiphased ceramic materials: processing and potential. Spark Plasma Sintering: A Promising New Technique and its Mechanism. Springer.

Heimann, R. B. (2010). Classic and Advanced Ceramics: From Fundamental to Applications. John Wiley and Sons.

Heimke, G. (1990). Osseo-integrated Implants: Basics, materials, and joint replacements. Introduction to Alumina Ceramics, 6. CRC Press.

Horn, D. S., Messing, G. L. (1995). Anisotropic grain growth in TiO_2-doped alumina. Materials Science and Engineering A195 (1995) 169-178.

Hosokawa, M. (2007). Nanoparticle technology handbook: Structure control of nanoparticle collectives by sintering and bonding. Elsevier.

Hsu, Y. F. (2005). Influence of Nb2O5 additive on the densification and microstructural evolution of fine alumina powders. Materials Science and Engineering A 399 (2005) 232–237

Jacobs, J. J., & Craig, T. L. (1998). Alternative bearing surfaces in total joint replacement. Mechanical Chracteristics. ASTM International.

Kang, S. J. L. (2005). Sintering: densification, grain growth, and microstructure.: Thermal Cycle and Microstructure Development. Butterworth-Heinemann, 2005

Koch, C. C. (2002). Nanostructured materials: processing, properties and potential applications Nanocrystalline Powders Consolidation Methods. William Andrew Publishing.

Koizumi, M., & Nishihara, M. (1991). Isostatic pressing: technology and applications. Methods of Hot Isostatic Pressing. Springer.

Kyocera Corporation. (2010). Typical Forming Process of Fine Ceramics. Retrieved, 24th August, 2010, from http://global.kyocera.com/fcworld/first/process04.html

Lee, W. E., & Rainforth, W. M. (1994). Ceramic microstructures: property control by processing. Alumina Polymorph and Crystal Structures, 266. Springer.

Lide, D. R. (2004). CRC Handbook Chemistry and Physics (85th ed). United States: CRC Press LLC.

Maca, K., Pouchly, V., Zalud, P. (2009). Two-Step Sintering of oxide ceramics with various crystal structures. Journal of the European Ceramic Society 30 (2010) 583–589.

Marucus, H. L. & Fine, M. E. (1972) Grain Boundary Segregation in MgO-Doped A120. J. Am. Ceram. Soc., 55 [l I 1568-70 (1972).

Martin, J. W. (2007). Concise encyclopedia of the structure of materials. Properties of Single Crystal Alumina, 23. Elsevier.

Menezesa, R. R., & Kiminamib, R.H.G.A. (2008). Microwave sintering of alumina–zirconia nanocomposites. Journal of materials processing technology 203 (2008) 513–517. Elsevier.

Ohji, T., & Singh, M. (2009). Advanced Processing and Manufacturing Technologies for Structural and Multifunctional Materials III, 19-22. John Wiley and Sons.

Oghbaei, M., & Mirzaee, O. (2010). Microwave versus conventional sintering: A review of fundamentals, advantages and applications. Journal of Alloys and Compounds 494 (2010) 175–189.

Olevsky, E.A., & Bordia, R. (2009). Advances in sintering science and technology. International Conference on Sintering 2009. John Wiley and Sons, 2009.

Peelamedu, R., Badzian, A., Roy, R., Martukanitz, R.P. (2004). Sintering of zirconia nanopowder by microwave-laser hybrid process. J. Am. Ceram. Soc. 87, 1806–1809.

Pfeifer, M. (2009). Materials enabled designs: The materials engineering perspective to product design and manufacturing. Butterworth-Heinemann

Rice, R. W., Dekker, M., Ebooks Corporation (2000) Mechanical Properties of Ceramics and Composites: Grain and Particle Effects. CRC Press.

Rice, R. W. (2003). Ceramic fabrication technology. Preparation of Ceramic Powders, 32. CRC Press.

Richerson, D. W. (2006). Modern ceramic engineering: properties, processing, and use in design, Volume 2005. CRC Taylor & Francis.

Riedel, R., & Chen, I. W. (2000). Ceramics Science and Technology: Properties, Volume 2. Chapter 1: Ceramics Oxides, 12. Wiley-VCH.

Reh, H. (2007). Current Classification of Ceramic Maaterials. Extrusion in ceramics. Springer, 2007.

Roush, M. L., & Webb, W. M. (2000). Applied reliability engineering. RIAC.

Salamon, D., & Shen, Z. (2007). Pressure-less spark plasma sintering of alumina. Materials Science and Engineering A 475 (2008) 105–107. Elsevier.

Satterfield, C. N. (1980), Heterogeneous Catalysis in Practice. McGraw-Hill, New York.

Segal, D. (1989). Chemical Synthesis of Advanced Ceramic Materials. University of Cambridge: Press Syndicate, 25-27.

Shackelford, J. F. (2009). Introduction to materials science for engineers. Prentice Hall, 2009

Smothers, W. J. & Reynolds, H. J. (1954). Sintering and Grain Growth of Alumina. Journal of The American Ceramic Society. Vol. 37, No. 12.

Society for Mining, Metallurgy, and Exploration (U.S.). (2006). Industrial minerals & rocks: commodities, markets, and uses, 241. SME Publishing.

Souto, P.M., Menezes, R.R., Kiminami, R.H.G.A. (2007). Microwave hybrid sintering of mullite powders. Am. Ceram. Soc. Bull. 86, 9201–9206.

Toy, C., Demirci, M., Onurlu, S., Tasar, M. S., Baykara, T. (1995). A colloidal method for manganese oxide addition to alumina powder and investigation of properties. Journal of Materials Science 30 (1995) 4183-4187.

Wang, C. J., Huang, C. Y., Wu, Y. C. (2009). Two-step sintering of fine alumina–zirconia ceramics. Ceramics International, 35, 1467-1472.

Wang, F. F. Y. (1976). Ceramic fabrication processes, Volume 9. Academic Press.

Yadoji, P., Peelamedu, R., Agrawal, D., Roy, R. (2003). Materials Science and Engineering B 98, 269–278.

Zavaliangos, A., & Laptev, A. (2001). Recent developments in computer modeling of powder metallurgy processes. IOS Press.

APPENDICES

APPENDIX A: Experimental Data

Bulk Density (g/cm³) for bars @ by using Water Immersion Technique

Temperature (°C)	Concentration of TiO$_2$ (wt.%)				
	0 wt%	0.5 wt%	1.5 wt%	3.0 wt%	5.0 wt%
1250	3.653	3.647	3.696	3.715	3.733
1350	3.648	3.683	3.737	3.766	3.781
1450	3.673	3.822	3.812	3.806	3.811

Relative Density (%) for bars by using Water Immersion Technique

Temperature (°C)	Concentration of TiO$_2$ (wt.%)				
	0 wt%	0.5 wt%	1.5 wt%	3.0 wt%	5.0 wt%
1250	91.78	91.63	92.86	93.34	93.79
1350	91.66	92.54	93.89	94.62	95.00
1450	92.29	96.03	95.78	95.63	95.75

Average Grain Size (µm) by using Linear Interpolation Technique

Temperature (°C)	Concentration of TiO$_2$ (wt.%)				
	0 wt%	0.5 wt%	1.5 wt%	3.0 wt%	5.0 wt%
1250	0.17	0.17	0.35	0.22	0.22
1350	0.18	0.44	0.45	0.42	0.59
1450	0.37	0.98	1.03	0.79	0.88

Average Largest Grain Size (µm) by using Linear Interpolation Technique

Temperature (°C)	Concentration of TiO$_2$ (wt.%)				
	0 wt%	0.5 wt%	1.5 wt%	3.0 wt%	5.0 wt%
1250	0.40 ± 0.08	0.40 ± 0.02	1.22 ± 0.24	0.66 ± 0.12	0.57 ± 0.10
1350	0.38 ± 0.02	0.87 ± 0.12	1.39 ± 0.45	1.31 ± 0.07	2.29 ± 0.67
1450	1.18 ± 0.13	2.33 ± 0.22	2.48 ± 0.46	2.21 ± 0.26	2.41 ± 0.42

Young's Modulus (GPa) by using original formula using mass in air

Temperature (°C)	Concentration of TiO_2 (wt.%)				
	0 wt%	0.5 wt%	1.5 wt%	3.0 wt%	5.0 wt%
1250	21.55	20.61	38.75	43.83	37.60
1350	36.00	71.75	99.80	96.39	93.81
1450	49.43	267.74	211.09	180.26	177.00

Vickers Hardness by using Microhardness Tester

Temperature (°C)	Concentration of TiO_2 (wt.%)				
	0 wt%	0.5 wt%	1.5 wt%	3.0 wt%	5.0 wt%
1250	0.74	2.00	1.20	1.30	1.35
1350	0.67	1.81	2.87	2.99	2.66
1450	1.79	7.60	6.61	5.34	6.64

Average Shrinkage of Al_2O_3 doped with different TiO_2 Composition (%)

Temperature (°C)	Concentration of TiO_2 (wt.%)				
	0 wt%	0.5 wt%	1.5 wt%	3.0 wt%	5.0 wt%
1250	5.10	5.35	7.75	8.80	8.60
1350	8.55	14.85	14.95	14.65	15.10
1450	10.50	22.50	21.10	20.55	20.35

APPENDIX B: Card Data of the Base Material, Additive and Secondary Phase

Aluminium Oxide, Corundum (Al$_2$O$_3$)

d-Spacings

λ=1.54056

— 00-010-0173 (Fixed Slit Intensity)
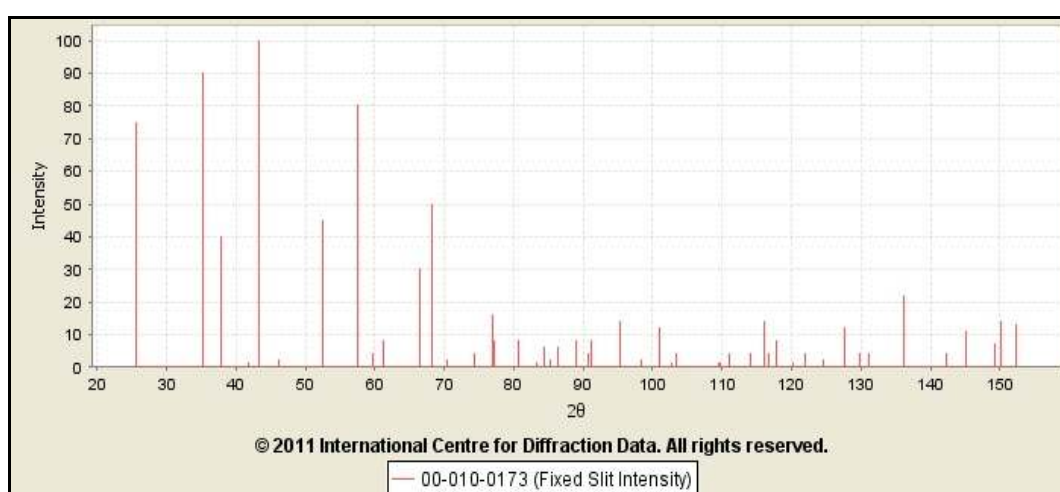
00-010-0173 (Fixed Slit Intensity)

2θ	d(Å)	Intensity	h	k	l	*
25.5835	3.479000	75	0	1	2	
35.1355	2.552000	90	1	0	4	
37.7838	2.379000	40	1	1	0	
41.6834	2.165000	<1	0	0	6	
43.3620	2.085000	100	1	1	3	
46.1829	1.964000	2	2	0	2	
52.5512	1.740000	45	0	2	4	
57.5175	1.601000	80	1	1	6	
59.7675	1.546000	4	2	1	1	
61.1638	1.514000	6	1	2	2	
61.3437	1.510000	8	0	1	8	
66.5468	1.404000	30	2	1	4	

68.1963	1.374000	50	3	0	0	
70.3569	1.337000	2	1	2	5	
74.2662	1.276000	4	2	0	8	
76.8800	1.239000	16	1	0	10	
77.2267	1.234300	8	1	1	9	
80.6919	1.189800	8	2	2	0	
83.2164	1.160000	<1	3	0	6	
84.3755	1.147000	6	2	2	3	
85.1811	1.138200	2	1	3	1	
86.3751	1.125500	6	3	1	2	
86.4611	1.124600	4	1	2	8	
89.0176	1.098800	8	0	2	10	
90.6620	1.083100	4	0	0	12	
91.2011	1.078100	8	1	3	4	
95.2600	1.042600	14	2	2	6	
98.4066	1.017500	2	0	4	2	
101.0920	0.997600	12	2	1	10	
102.7880	0.985700	<1	1	1	12	
103.3450	0.981900	4	4	0	4	
109.5220	0.943100	<1	3	2	1	
109.8330	0.941300	<1	1	2	11	
111.0290	0.934500	4	3	1	8	
114.1260	0.917800	4	2	2	9	
116.1410	0.907600	14	3	2	4	
116.6300	0.905200	4	0	1	14	
117.9020	0.899100	8	4	1	0	
120.2330	0.888400	<1	2	3	5	
122.0710	0.880400	4	4	1	3	
124.6460	0.869800	2	0	4	8	
127.7310	0.858000	12	1	3	10	
129.9160	0.850200	4	3	0	12	
131.1480	0.846000	4	2	0	14	
136.1620	0.830300	22	1	4	6	
142.3960	0.813700	4	1	1	15	
145.2080	0.807200	11	4	0	10	
149.2870	0.798800	7	0	5	4	
150.2440	0.797000	14	1	0	16	
152.4450	0.793100	13	3	3	0	

Titanium Oxide, Anatase (TiO₂)

d-Spacings

λ=1.54056

— 00-021-1272 (Fixed Slit Intensity)
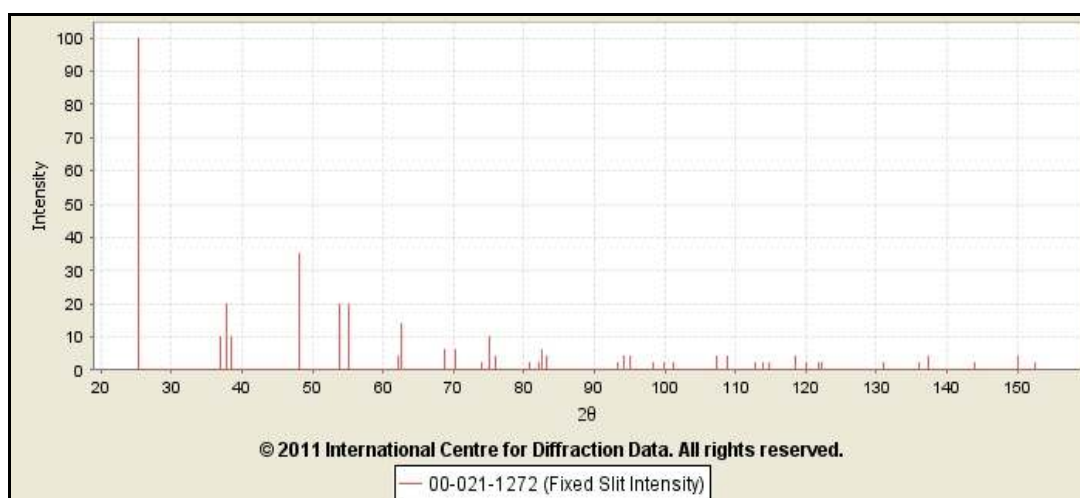
00-021-1272 (Fixed Slit Intensity)

2θ	d(Å)	Intensity	h	k	l	*
25.2806	3.520000	100	1	0	1	
36.9459	2.431000	10	1	0	3	
37.8002	2.378000	20	0	0	4	
38.5750	2.332000	10	1	1	2	
48.0487	1.892000	35	2	0	0	
53.8897	1.699900	20	1	0	5	
55.0602	1.666500	20	2	1	1	
62.1189	1.493000	4	2	1	3	
62.6885	1.480800	14	2	0	4	
68.7601	1.364100	6	1	1	6	
70.3088	1.337800	6	2	2	0	
74.0290	1.279500	<2	1	0	7	
75.0294	1.264900	10	2	1	5	
76.0172	1.250900	4	3	0	1	
80.7252	1.189400	<2	0	0	8	
82.1364	1.172500	2	3	0	3	
82.6595	1.166400	6	2	2	4	
83.1465	1.160800	4	3	1	2	
93.2174	1.060000	2	2	1	7	

94.1782	1.051700	4	3	0	5	
95.1396	1.043600	4	3	2	1	
98.3150	1.018200	2	1	0	9	
99.8007	1.007000	2	2	0	8	
101.2180	0.996700	2	3	2	3	
107.4440	0.955500	4	3	1	6	
108.9590	0.946400	4	4	0	0	
112.8360	0.924600	<2	3	0	7	
113.8570	0.919200	2	3	2	5	
114.9040	0.913800	2	4	1	1	
118.4340	0.896600	4	2	1	9	
120.0990	0.889000	2	2	2	8	
121.7200	0.881900	<2	4	1	3	
122.3300	0.879300	2	4	0	4	
131.0290	0.846400	2	4	2	0	
135.9910	0.830800	<2	3	2	7	
137.3840	0.826800	4	4	1	5	
143.8780	0.810200	2	3	0	9	
150.0280	0.797400	4	4	2	4	
152.6220	0.792800	2	0	0	12	

Titanium Oxide, Rutile (TiO$_2$)

d-Spacings

λ=1.54056

— 00-021-1276 (Fixed Slit Intensity)
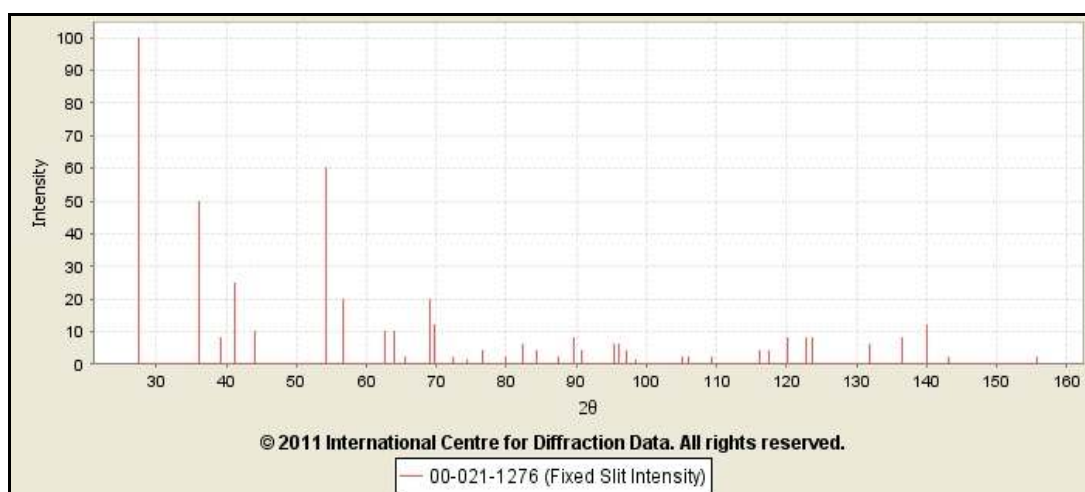
00-021-1276 (Fixed Slit Intensity)

2θ	d(Å)	Intensity	h	k	l	*
27.4460	3.247000	100	1	1	0	
36.0850	2.487000	50	1	0	1	
39.1866	2.297000	8	2	0	0	
41.2252	2.188000	25	1	1	1	
44.0504	2.054000	10	2	1	0	
54.3216	1.687400	60	2	1	1	
56.6403	1.623700	20	2	2	0	
62.7406	1.479700	10	0	0	2	
64.0383	1.452800	10	3	1	0	
65.4782	1.424300	2	2	2	1	
69.0082	1.359800	20	3	0	1	
69.7880	1.346500	12	1	1	2	
72.4075	1.304100	2	3	1	1	
74.4089	1.273900	1	3	2	0	
76.5076	1.244100	4	2	0	2	
79.8193	1.200600	2	2	1	2	
82.3323	1.170200	6	3	2	1	
84.2575	1.148300	4	4	0	0	
87.4609	1.114300	2	4	1	0	

89.5544	1.093600	8	2	2	2	
90.7049	1.082700	4	3	3	0	
95.2720	1.042500	6	4	1	1	
96.0140	1.036400	6	3	1	2	
97.1731	1.027100	4	4	2	0	
98.5109	1.016700	<1	3	3	1	
105.0950	0.970300	2	4	2	1	
106.0150	0.964400	2	1	0	3	
109.4020	0.943800	2	1	1	3	
116.2220	0.907200	4	4	0	2	
117.5220	0.900900	4	5	1	0	
120.0540	0.889200	8	2	1	3	
122.7830	0.877400	8	4	3	1	
123.6550	0.873800	8	3	3	2	
131.8400	0.843700	6	4	2	2	
136.5420	0.829200	8	3	0	3	
140.0440	0.819600	12	5	2	1	
143.1080	0.812000	2	4	4	0	
155.8550	0.787700	2	5	3	0	

Aluminium Titanate (Al$_2$TiO$_5$)

d-Spacings

λ=1.54056

— 00-041-0258 (Fixed Slit Intensity)
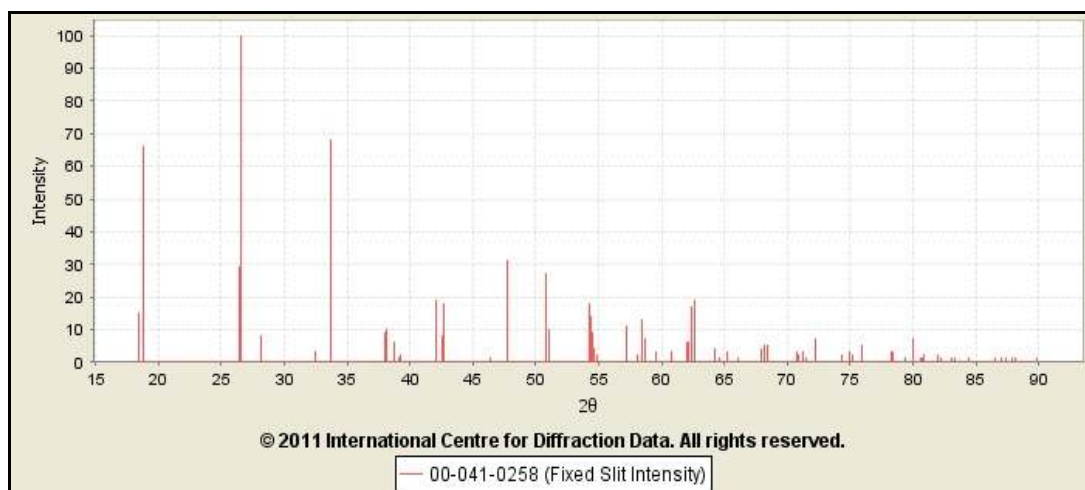
00-041-0258 (Fixed Slit Intensity)

2θ	d(Å)	Intensity	h	k	l	*
18.3935	4.819500	15	0	2	0	
18.8001	4.716200	66	2	0	0	
26.3986	3.373400	29	2	2	0	
26.5235	3.357800	100	1	0	1	
28.1154	3.171200	8	1	1	1	
32.4840	2.754000	3	1	2	1	
33.7242	2.655500	68	2	3	0	
37.9826	2.367000	9	3	0	1	
38.1046	2.359700	10	4	0	0	
38.7565	2.321500	6	1	3	1	
39.1547	2.298800	1	3	1	1	
39.2739	2.292100	2	4	1	0	
42.0474	2.147100	19	2	4	0	
42.5079	2.124900	8	3	2	1	
42.6277	2.119200	18	4	2	0	
46.3118	1.958830	1	1	4	1	
47.6669	1.906260	15	3	3	1	
47.7728	1.902280	31	4	3	0	
50.7947	1.795970	27	0	0	2	

51.1066	1.785740	10	2	5	0	
54.2704	1.688870	18	3	4	1	
54.3474	1.686660	14	4	4	0	
54.4596	1.683450	9	0	2	2	
54.6194	1.678900	4	2	0	2	
54.8314	1.672910	2	1	5	1	
57.2503	1.607840	11	0	6	0	
58.1254	1.585700	2	2	2	2	
58.3964	1.578980	13	5	2	1	
58.6342	1.573140	7	6	0	0	
59.4885	1.552580	3	6	1	0	
60.8103	1.521960	3	2	6	0	
62.0015	1.495550	6	6	2	0	
62.0015	1.495550	6	3	5	1	
62.0886	1.493660	6	4	5	0	
62.3464	1.488100	17	2	3	2	
62.5865	1.482970	19	5	3	1	
64.1764	1.450010	4	1	6	1	
64.6422	1.440680	1	0	4	2	
65.2060	1.429580	3	4	0	2	
66.0626	1.413110	1	6	3	0	
67.9780	1.377880	4	2	4	2	
68.1974	1.373980	5	5	4	1	
68.3974	1.370450	5	4	2	2	
70.7821	1.330010	3	3	6	1	
70.8611	1.328720	2	4	6	0	
71.2169	1.322950	3	2	7	0	
71.5498	1.317610	<1	6	4	0	
72.2798	1.306090	7	4	3	2	
74.3361	1.274970	2	1	7	1	
74.9125	1.266580	3	2	5	2	
75.1486	1.263190	2	5	5	1	
75.2019	1.262430	2	7	0	1	
75.9713	1.251540	5	7	1	1	
78.2053	1.221290	3	7	2	1	
78.3617	1.219240	3	6	5	0	
79.4005	1.205880	<1	0	8	0	
80.0233	1.198050	7	0	6	2	

80.5957	1.190980	1	3	7	1
80.6719	1.190050	1	4	7	0
80.8403	1.187990	2	1	0	3
81.9324	1.174900	2	7	3	1
81.9324	1.174900	2	6	1	2
82.2521	1.171140	1	8	1	0
83.1018	1.161310	1	2	6	2
83.3350	1.158650	1	5	6	1
84.4597	1.146070	1	8	2	0
86.4765	1.124440	<1	6	6	0
87.0529	1.118470	1	7	4	1
87.4385	1.114530	1	1	3	3
87.8207	1.110660	1	6	3	2
88.1203	1.107660	<1	8	3	0
89.8994	1.090300	<1	3	2	3

APPENDIX C: Gantt Chart and Flow Chart of Final Year Project

Gantt Chart for Project Part I

Week / Task Name	1	2	3	4	5	6	7	8	9	10	11	12	13	14	15
Title Selection	▨	▨													
Literature Review		▨	▨	▨	▨	▨	▨	▨	▨	▨	▨	▨	▨		
Ceramics Studies		▨	▨	▨	▨										
Alumina Ceramics Studies						▨	▨	▨	▨	▨	▨	▨			
Methodology Studies											▨	▨			
Chapter 1				▨											
Chapter 2					▨	▨	▨								
Chapter 3								▨	▨	▨	▨	▨			
Chapter 4											▨	▨	▨		
Weekly Report							▨	▨	▨	▨	▨	▨			
Oral Presentation 1														▨	▨

Gantt Chart for Project Part II

Week / Task Name	1	2	3	4	5	6	7	8	9	10
Preparation TiO$_2$ doped alumina powder	▨	▨	▨	▨						
Body Preparation and Sintering Process				▨	▨	▨	▨			
Body Characterization and Testing							▨	▨	▨	▨

Gantt Chart for Project Part III

Week / Task Name	1	2	3	4	5	6	7	8	9	10	11	12	13	14	15	16	17	18
Analysis of Data	▨	▨	▨	▨	▨													
Thesis Writing	▨	▨	▨	▨	▨	▨	▨	▨	▨	▨	▨	▨	▨	▨	▨	▨	▨	▨
Chapter 5		▨	▨	▨	▨													
Chapter 6						▨	▨	▨	▨	▨	▨							
Thesis (First Draft)												▨	▨					
Final Thesis														▨	▨	▨	▨	▨
Oral Presentation 2														▨	▨			

Flowchart

```
┌─────────────────────────────┐
│  Extensive Literature Review │
└─────────────────────────────┘
              │
              ▼
┌─────────────────────────────┐
│      Study on Ceramics       │
└─────────────────────────────┘
              │
              ▼
┌─────────────────────────────┐
│   Study on Alumina Ceramics  │
└─────────────────────────────┘
              │
              ▼
┌─────────────────────────────┐
│     Study on Methodology     │
└─────────────────────────────┘
              │
              ▼
┌──────────────────────────────────────┐
│ Preparation of TiO₂ – doped alumina   │◄──┐
│ powder                                 │   │
└──────────────────────────────────────┘   │
              │                              │
              ▼                              │
┌─────────────────────────────┐             │
│  Body Preparation and        │            │
│  Sintering                   │            │
└─────────────────────────────┘            │
              │                              │
              ▼                              │
┌─────────────────────────────┐             │
│ Body Characterization and    │            │
│ Testing                      │            │
└─────────────────────────────┘            │
              │                              │
              ▼                              │
┌─────────────────────────────┐             │
│      Analysis of Data        │            │
└─────────────────────────────┘            │
              │                              │
              ▼                              │
           ◇ OK ?  ──── No ─────────────────┘
              │
             Yes
              │
              ▼
┌─────────────────────────────┐
│       Thesis Writing         │
└─────────────────────────────┘
```

Preparation of TiO_2 – doped alumina powder